（千葉大学学位申請論文）

ピッチ系活性炭素繊維の調製と気体吸着特性

２０１３年1月

千葉大学大学院理学研究科

基盤理学専攻化学コース

中東　義貴

Contents

1. General Introduction

In today's society, efforts are being made to improve the global environment, but its condition is still worsening. Since the nuclear accident, Japanese energy consumption has become even more dependent on fossil fuels, and there has been an increase in the carbon dioxide emissions which are thought to be the main cause of global warming. Regarding measures to combat global warming in particular, regulations are being established to limit emissions, but measures to remove emitted substances which cause warming are an important topic, and many techniques for this purpose are being implemented or tested. There is increasing international awareness of the effectiveness of carbon capture and storage (CCS) as a method for reducing emissions of the carbon dioxide which causes warming, and CCS is playing an important role.

Here, CCS refers to the process of artificially capturing CO_2, either after or immediately before it would be released into the atmosphere as a gas, and storing it by containing it in the ground or underwater.

R&D is being conducted on the following methods for separation and capture in this field:

The chemical adsorption method in the field of CO_2 separation and capture technology is a separation/capture method using an alkaline solution of amines or other chemicals. When an amine group is used, amine carbonate is formed due to a binding reaction with CO_2. CO_2 is separated from this produced amine carbonate. A large amount of energy is needed in this separation process. In the physical adsorption method, CO_2 is selectively

adsorbed to an adsorbent such as activated carbon or zeolite, and the PSA method is the primary method used for separation and capture. This method selectively separates and captures CO_2 by varying pressure. The zeolite used as an adsorbent has high adsorption selectivity for CO_2. However, high levels of energy are needed to separate and capture CO_2 by this method. In the field of activated carbon, R&D is being conducted on using various materials as adsorbents, and an actual track record of use has been established.

This paper looks at these activated carbon adsorbents, and reports on the results of research on activated carbon fibers, whose pore structure is extremely monodispersed. The research aims to obtain basic data useful for capture and storage of CO_2.

2. Activated carbon fiber

2-1. What is activated carbon fiber?

Activated carbon fiber is a material which has the functionality of activated carbon, exemplified by adsorption, and the morphological characteristics of a fiber. Its development history is extremely short compared to conventional materials such as granular activated carbon. According to a literature survey of patents and other documents, it can be thought that this material was commercialized in the 1970s.

At present, companies in Japan are the main firms manufacturing this material. Also, among manufacturers, there are few whose main business is producing conventional activated carbon, and most are fiber manufacturers who did not enter the business from the raw material side. Furthermore, there have been reports in recent years that this material is being produced in China. Based on the size of the market, the scale of production is a few hundred tons.

Generally speaking, activated carbon is used in a wide range of fields in either powdered or granular form. However, activated carbon fibers can be used both in applications where conventional activated carbon is used, and in many other applications. Activated carbon fibers have the characteristics of a fibrous shape, i.e., the ability to provide maximal use of specific surface area, and also demonstrate outstanding workability in areas such as fabricating composites with other materials by applying fiber processing technology. Because of these characteristics, activated carbon fibers are used in a broad variety of fields, including everything from electronic devices,

which use the high specific surface area of activated carbon fiber, to systems such as solvent recovery plants which employ the fiber's rapid adsorption-desorption rate.

2-2. Raw materials and preparation

Raw materials

The following are the raw materials for activated carbon fibers in current industrial production.

Organic fiber types

1. Phenol resin

Fiberization is achieved as phenolic novolac fiber, and manufacturing is performed from a fiber developed in the US as a flame-resistant fiber.

2. Acrylic resin

In general, this is manufactured from polyacrylonitrile, which is the same raw material as that for PAN-based carbon fiber.

3. Cotton, rayon

These are manufactured from cellulose fibers.

Inorganic fiber type

1. Coal pitch

This is manufactured using pitch as a raw material. This pitch is obtained from coal tar by using a polymerization reaction.

Preparation

In general, carbonization or stabilization is performed by raising the temperature, and then activation is performed, during which pores are formed.

The following compares the organic and inorganic fiber types.

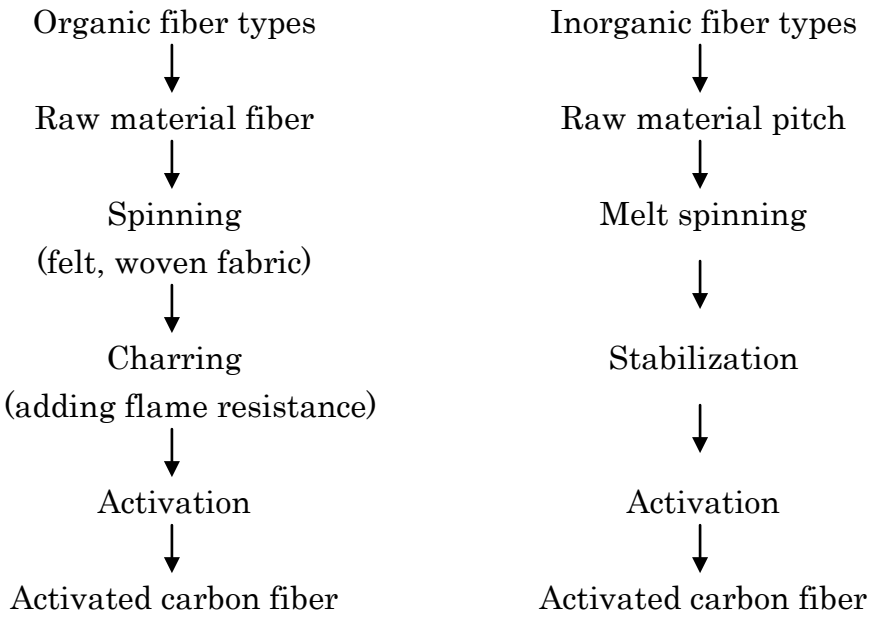

These two types differ in their treatment due to the different characteristics of their raw materials. With organic fiber types, either to perform carbonization or flame-resistance treatment is performed, while with the inorganic fiber type, stabilization is performed.

2-3. Basic characteristics

The basic characteristics of activated carbon fiber are morphology, pore distribution and specific surface area.

Morphology

These fibers have a smooth surface, and the outer surface area is extremely large compared to granular activated carbon. This is reflected in the high adsorption rate.

Pore size distribution

Whereas activated carbon fiber is monodispersed, primarily with micropores, activated carbon is polydispersed, with various pores. This is thought to be because there are fewer impurities necessary for synthesizing micropores since there is thorough pre-treatment when the raw material is prepared. Fig. 2-1 schematically indicates models of pore structure, based on the results of observation using electron micrographs and pore measurement.

Factors which affect adsorption function of activated carbon have a strong dependence on pore structure. The classification of pore diameter shown in Table 2-1 was internationally established by IUPAC in 1972.

Table 2-1. Classification of pores

name	pore diameter
micropore	＜２ｎｍ
mesopore	２～５０ｎｍ
marcopore	５０ｎｍ＜

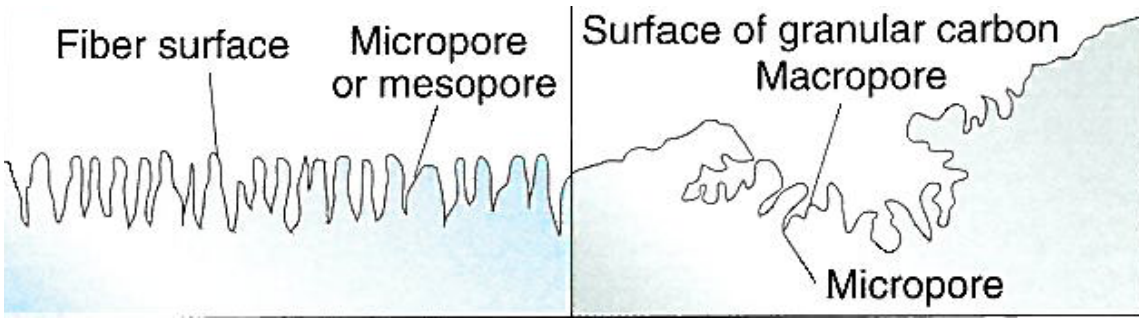

Activated carbon fiber granular activated carbon

Fig. 2-1: Pore structure models for activated carbon fiber and granular activated carbon

Based on previous structural analysis and measurement results, the following facts are known about the pore structure of activated carbon fiber.

1) There are no macropores.

2) Micropores are the main constituent, and comprise the majority of the specific surface area.

3) As specific surface area increases, so does the average diameter and volume of pores.

3. Pitch-based activated carbon fiber

3-1. Raw material

The raw material pitch is an aromatic compound obtained through a polycondensation reaction on coal tar by heat treatment. The coal tar is obtained as a byproduct when coke is manufactured by carbonizing coal in a coke oven.

Fig. 3-1 shows a schematic diagram illustrating the principles of a coke oven.

Fig. 3-1: Coke oven principles

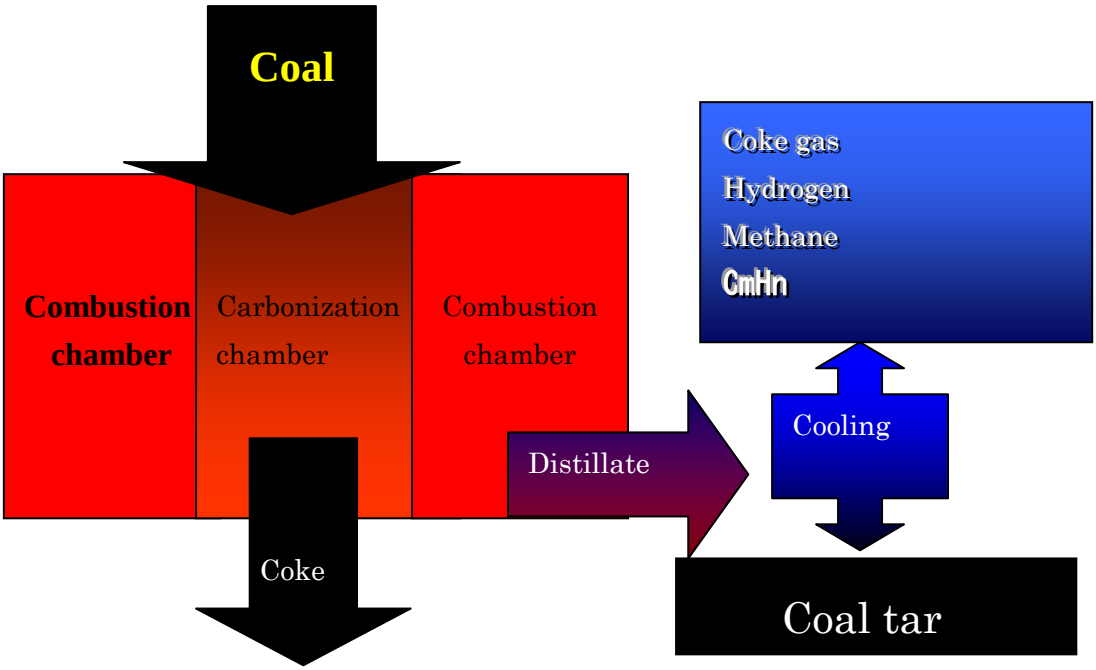

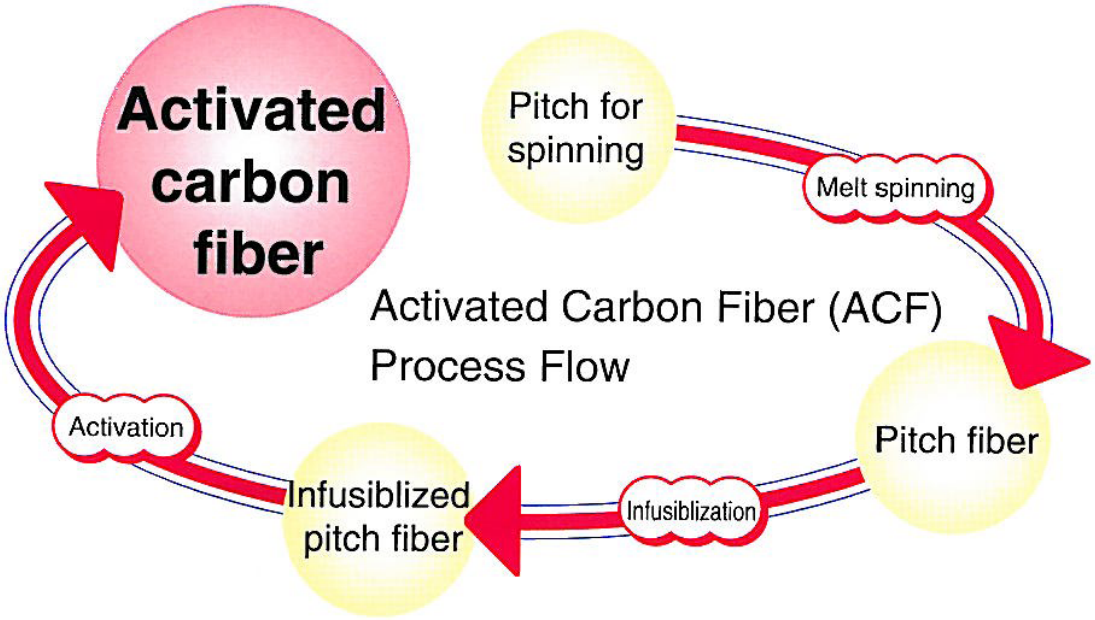

Fig. 3-2 Method of preparing pitch-based activated carbon fiber

3-2. Preparation

Fig. 3-2 shows the method of preparing pitch-based activated carbon fiber. The above process employs the following three basic technologies:

1) Melt spinning of raw material pitch

2) Stabilization of pitch fiber

3) Activation of stabilized fiber

Melt spinning of pitch is based on technology for synthetic fiber, and is enhanced to suit the characteristics of the raw material pitch.

Stabilization is a type of treatment in which, because pitch fiber melts in the presence of heat, intermolecular-cross-linking is promoted in an atmosphere containing oxygen, while controlling the temperature. This stabilization treatment affects the yield up to finishing of the final product, as well as performance of the product, and is therefore the most important treatment step in the preparation process for pitch-based activated carbon

fiber. Fig. 3-3 shows the change in weight of pitch fiber during stabilization.

Stabilization is a partial oxidation/cross-linking reaction in hot air, and an increase in weight is seen due to oxygen cross-linking as the temperature rises.

In the case of ordinary activated carbon, both the gas and chemical activation methods are used for the final activation process, while the gas activation method is primarily used for activated carbon fiber.

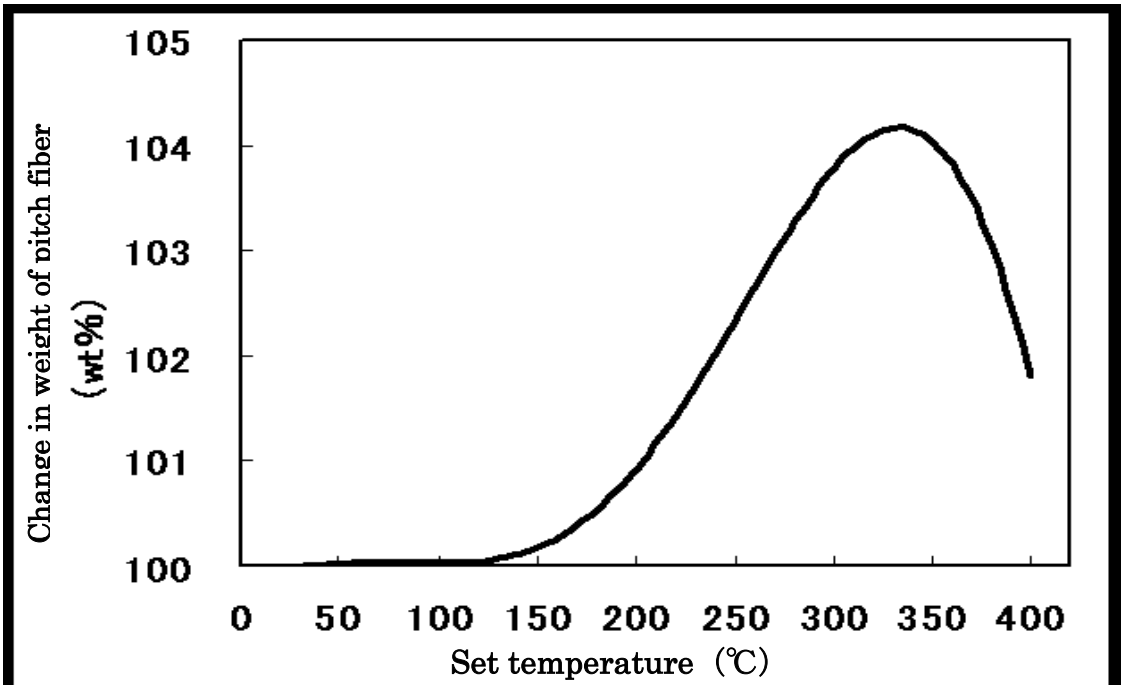

Fig. 3-3: Change in weight of pitch fiber during stabilization treatment

In the activation process, the contained carbon is gasified due to a hydrogen gasification reaction, thereby opening pores and providing functionality as active carbon. In this process, activated carbon fibers with varying specific surface area and adsorption performance are produced by adjusting the temperature, treatment time and steam concentration. In actual manufacturing, setting to manufacturing conditions is done under

constant steam concentration based on temperature and time data.

3-3. Basic characteristics

In addition to the characteristics described in Section 2-3, pitch-based activated carbon fiber also has the following characteristics.

1) High theoretical carbonization yield (can be manufactured at low cost).

2) High carbon content.

3) Can be processed into various forms by exploiting fiber features.

The most important feature is that fiber can be manufactured from pitch with high yield.

References

(1) *Activated Carbon Handbook*, Hayashi, Masahiko and Kawashita, Yuka, Maruzen Company, Limited, Jan. 31, 2011 (in Japanese)

(2) *Activated Carbon Fiber*, Shimada, Masayoshi, Tojusha Co., Ltd., Nov. 30, 1990 (in Japanese)

4. Basic Theory of Adsorption

4.1 Adsorption

Adsorption phenomenon is equilibrium phenomenon between the interfaces such as solid-liquid, solid-gas, and liquid-liquid. The model of adsorption between a solid-gas phase is shown in Fig. 4.1.1. In the case of the solid-gas phase, the adsorbed layer density near the solid surface is higher than the bulk density and gradually decreases to same as the bulk gas density when the distance from the solid surface becomes far. This phenomenon is widely used for the study on the state of the surface and nanostructure analysis in academic and for the material storage, separation, and catalysis in industry. Some of the principle terms associated with adsorption are defined in Table 4.1.1.

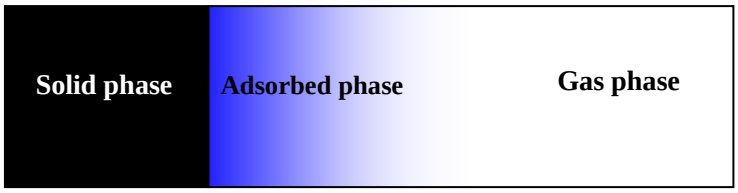

Fig. 4.1.1. The model of adsorption (solid-gas phase)

Table 4.1.1 Definition terms of adsorption [1]

Term	Definition
Adsorption	Enrichment of one or more components in an interfacial layer
Adsorbate	Substance in the adsorbed state
Adsorptive	Adsorbable substance in the fluid phase
Adsorbent	Solid material on which adsorption occurs

4.2 Physical adsorption and Chemical adsorption [2]

The adsorption phenomena are distinguished in physical and chemical adsorption.

Physical adsorption is caused by the interaction which is mainly the dispersion force between the surface and molecules and forms the multilayer because the interaction force works for a long distance (several nm). On the other hand, chemical adsorption is caused by the charge transfer interaction or chemical bond generation between the surface and molecules and confined to only a monolayer. Therefore, the properties of physical and chemical adsorption are different, as shown in Table 4.2.1. In this thesis, the adsorption indicates physical adsorption.

Table. 4.2.1. Comparison of physical and chemical adsorption [(2)]

	Physical adsorption	Chemical adsorption
Adsorption amount	> monolayer capacity	< monolayer
Adsorpiton rate	quick	slow
Heat of adsorption	< 100 kJ /mol	> 100 kJ / mol
Specific interaction	none	dominant
Reversibility	dominant	none

4.3 Intermolecular Interaction

The interaction occurs between closed shell molecules, which are intermolecular interaction. The intermolecular interaction mainly is caused by attractive and repulsive forces. The forces for physical adsorption always include the dispersion attractive interactions and the short-range repulsion. In the case of same molecules, the intermolecular forces is usually expressed by the 12-6 Lennard-Jones potential as shown here,

$$u_{ii(r)} = 4\varepsilon_{ii}\left\{\left(\frac{\sigma_{ii}}{r}\right)^{12} - \left(\frac{\sigma_{ii}}{r}\right)^{6}\right\} \tag{4.3.1}$$

where u_{ii} is the potential energy, r is the distance between molecules, and σ_{ii} and ε_{ii} are the Lennard-Jones size and energy parameters, respectively. On the other hand,

Lennard-Jones size and energy parameters are defined by Lorentz-Berthelot law in the case of the intermolecular interaction between different molecules, expressed by

$$\sigma_{ij} = \frac{1}{2}(\sigma_{ii} + \sigma_{jj}) \tag{4.3.2}$$

$$\varepsilon_{ij} = (\varepsilon_{ii}\varepsilon_{jj})^{1/2} \tag{4.3.3}$$

Then, the 12-6 Lennard-Jones potential is given in

$$u_{ij(r)} = 4\varepsilon_{ij}\left\{\left(\frac{\sigma_{ij}}{r}\right)^{12} - \left(\frac{\sigma_{ij}}{r}\right)^{6}\right\} \tag{4.3.4}$$

However, ε_{ij} determined by Lorentz-Berthelot law seems to overestimate. Therefore, a more accurate ε_{ij} determine by fitting of experimental data.

In the case of the interaction between the solid surface and a molecule, the adsorbed molecule interacts with each atoms of the solid. The molecule interaction is expressed by the summation of Lennard-Jones potential between molecule and each atoms of solid surface.

$$U_{(r)} = \sum u_{(r)} = \sum 4\varepsilon_{ij}\left\{\left(\frac{\sigma_{ij}}{r}\right)^{12} - \left(\frac{\sigma_{ij}}{r}\right)^{6}\right\} \tag{4.3.5}$$

Therefore, the interaction with solid - gas is larger than that with gas-gas. Accordingly, molecules condense to the solid surface. As the adsorbed density near the solid surface is higher than the bulk density, adsorption phenomenon occurs on the solid surface.

Nanopores have more enhance interaction than the solid surface. We assume that one solid surface get closer to another solid surface, which is called slit pore. Since slit pore has strong potential due to the summation of potential between solid surfaces, the adsorbed density in slit pore is far larger than that on the solid surface. The intermolecular interactions are summarized in Fig. 4.3.1. A pore is classified by pore width, shown in Table 4.3.1. The interaction potential changes by the nanopore size and

molecular size. Fig. 4.3.2 shows the potential difference of pore size obtained by 10-4-3 potential proposed by Steele [3].

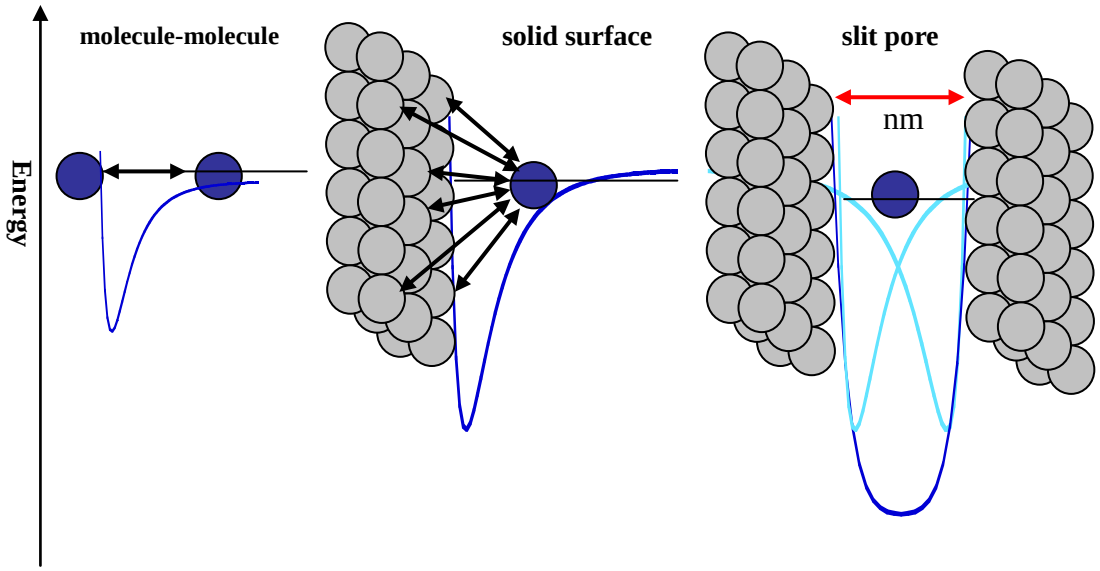

Fig. 4.3.1. Difference of potential depth with each interaction.

Table 4.3.1. The classification of pores [4]

	Pore size
ultramicropore	w < 0.7 nm
micropore	w < 2 nm
mesopore	2 nm < w < 50 nm
micropore	50 nm < w

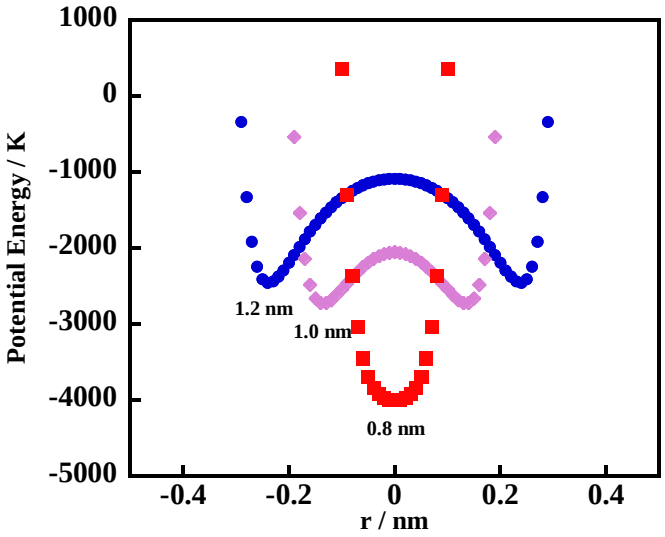

Fig. 4.3.2. The potential energy difference for pore width.

4.4 Adsorption Isotherm [1, 5]

The adsorption amount, n, on the solid surface depends on the measuring pressure, temperature, natures of the fluid and the solid. Thus, the adsorption amount can be expressed as

$$n = f(P, T, fulid, solid) \tag{4.4.1}$$

In general, the adsorption measurement carried out a function of pressure at constant temperature T, and then the equation can simply to

$$n = f(P)_{T,gas,solid} \tag{4.4.2}$$

This relation is called the adsorption isotherm. When the temperature is below the critical temperature, the equation is given by using saturate vapor pressure P_0

$$n = f(P / P_0)_{T,gas,solid} \tag{4.4.3}$$

where P/P_0 is relative pressure.

The phenomenon in which the adsorbate adsorbs on the interface is termed the adsorption. On the contrary, the phenomenon in which the adsorbate leaves from the

interface is termed the desorption. If the adsorption amounts of the adsorption process do not coincide with that of the desorption process, this phenomenon is called the hysteresis. The adsorption amount is always smaller than the desorption amount in the hysteresis region.

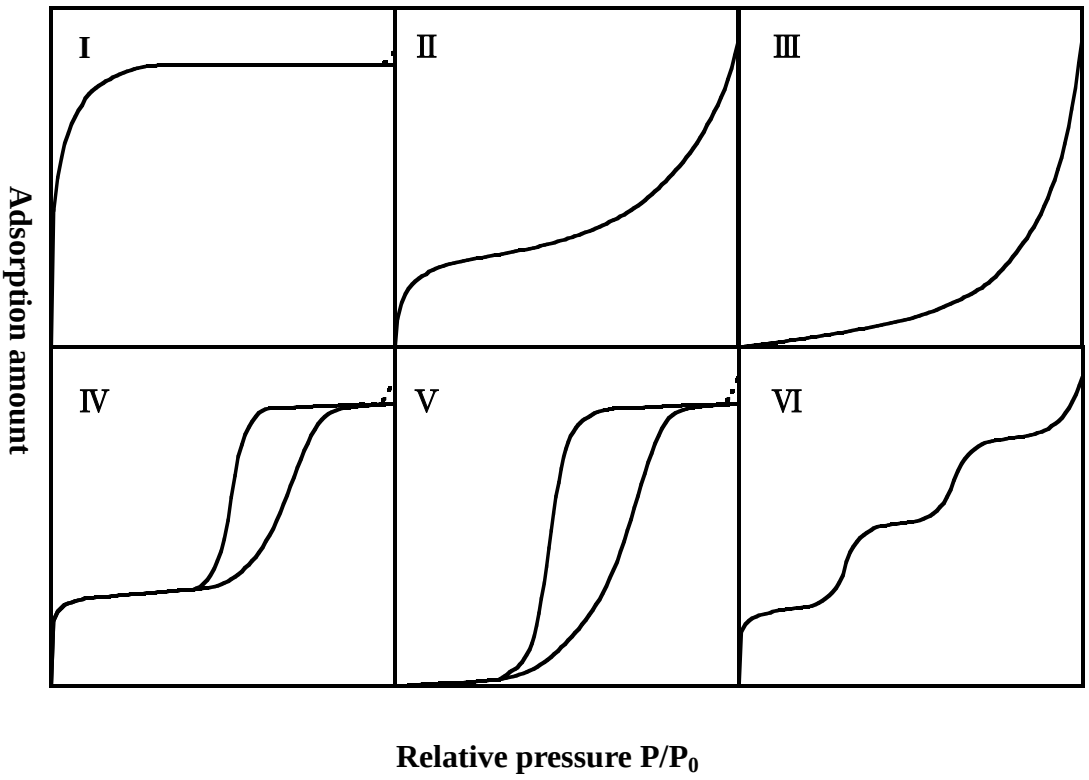

Fig. 4.4.1. Types of adsorption isotherms

Brunauer, Deming, Deming and Teller proposed a classification of the adsorption isotherms on the vapor into five types called BDDT classification in 1940 [6]. In addition, Sing proposed the step like adsorption isotherm [7] The classification of this six type adsorption isotherm on the vapor is accepted by the IUPAC shown in Fig. 4.4.1. Type I isotherm, which is called Langmuir isotherm, is concave to the relative pressure (P/P_0) axis and the adsorption amount approaches a limiting value as P/P_0 approaches 1. Type I isotherm is observed in chemical adsorption which is adsorbed only monolayer on the

surface. Type I isotherms are also observed in physical adsorption on microporous solid having relatively small external surfaces. As the adsorbed potential overlap from both of pore wall, the adsorption occurs from the low pressure region. This is called micropore filling. Type I isotherm indicates the strong interaction between adsorbent-adsorbate. The limiting uptake of adsorbate is governed by the micropore volume of the material.

Type II isotherm is obtained with a nonporous or macroporous adsorbent. This type of isotherm represents multilayer adsorption. It is explained by Brunauer, Enammet, and Teller. Therefore, Type II is called BET type. The knee of the Type Ⅱ isotherm, called Point B, is usually considered to represent the completion of a monolayer and beginning of the formation of the multilayer.

Type III isotherms are convex to the P/P_0 axis over its entire range. Type III isotherm is caused by stronger adsorbate-adsorbate than adsorbate-adsorbent interaction. This isotherm is shown in the adsorption of water on nonporous carbon materials.

Type IV isotherm is related to capillary condensation in mesopores, indicated by the steep uptake at higher relative pressures. The isotherm is observed with hysteresis loop. Type IV is similar to Type II except for existing of mesopores.

Type V isotherm is also related to capillary condensation in mesopores and observed with hysteresis loop. Type V is similar to Type III except for existing of mesopores. This isotherm is shown in the adsorption of water on micorporous carbon materials.

Type VI isotherm is called the step wise isotherm. This isotherm associated with layer-by-layer adsorption on an uniform non-porous solid. For example, this type isotherm is observed in the adsorption of Kr on the perfect graphite such as High Orientated Pyrolytic Graphite (HOPG).

In the case of supercritical gas adsorption, as the capillary condensation do not occur

in the supercritical state and the adsorbate-adsorbate interaction is weaker than adsorbate-adsorbent interaction due to the molecules having high energy, Type I or Type II isotherm can be observed [8]. However, the raw data of the adsorption isotherm differ from each isotherm because of the adsorbed-layer buoyancy. The adsorption isotherm has a maximum of the adsorption amount [9], which is called the surface excess mass as described next section.

4.5 Measurement Method of Adsorption Isotherm [1]

The measurement of an adsorption isotherm is carried out by mainly two methods, the gravimetric method and the volumetric method. These methods have advantages and disadvantages.

4.5.1 Volumetric Method [10,11]

The adsorption amount is obtained from the pressure change using the ideal gas equation or the van der Waals equation. The volumetric method apparatus is composed of the vacuum part, the gas reservoir, the sample cell, and the pressure measuring parts shown in Fig. 4.5.1. Although the apparatus of volumetric method is simple compared with that of gravimetric method, it is difficult to obtain the accurate adsorption amount because it is necessary to keep the temperature at constant and to measure the accurate dead and sample volumes. The ideal gas or van der Waals equations are not used for the calculation of the adsorption amount due to the error in the high-pressure adsorption. The most disadvantage of this method is that the volumetric method tends to increase the error every measured points.

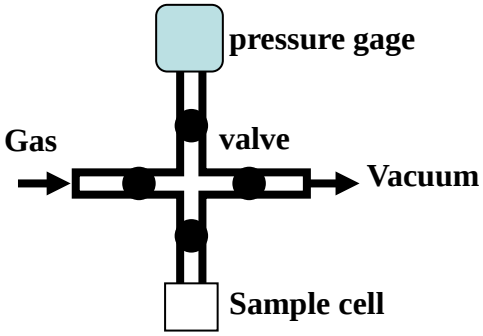

Fig.. 4.5.1. Diagram of volumetric method

4.5.2 Gravimetric Method [12]

The gravimetric method is the most exact measurement method because the measurement pressure and the adsorption amount are measured individually each measurement pressure. The apparatus of gravimetric method is composed of the vacuum part, the gas reservoir, and the weight and pressure measuring parts shown in Fig. 4.5.2. Although a quart spring is usually used for the measurement of adsorption amount, the electric microbalance or magnetic suspension microbalance is used for the more accurate measurement such as supercritical gas adsorption [13-16]. However, the buoyancy correction of the sample, determined by the particle density, is needed to the high-pressure gas adsorption.

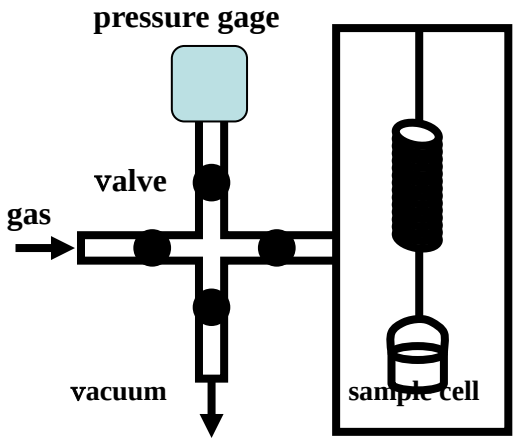

Fig. 4.5.2. Diagram of gravimetric method

4.6 Particle Density of the Sample

A particle density is important for obtaining true adsorption amount because the buoyancy correction of the sample and the determination of the accurate dead volume for the gravimetric and volumetric method, respectively [8,17,18]. The particle density

differs from the true density determined by XRD and the packing density. The particle density ρ_s takes account for the volume of the material it self and the closed pore [19]. The particle density is expressed as

$$\rho_s = \frac{m}{V_s + V_{close}} \tag{4.6.1}$$

where m is the mass of the solid, V_s and V_{close} are the volume of the solid and the closed pore, respectively. The pore model is shown in Fig. 4.6.1. The particle density is obtained from the buoyancy curve using He under high-pressure [13]. However, as the molecular size is different for each molecule, the particle density might be changed with the adsorptive molecule. In chapter 5, the determination method of accurate particle density is described.

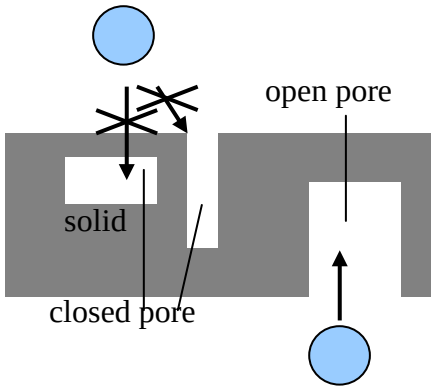

Fig. 4.6.1. Model of closed pore and open pore from the view of molecule

4.7 Pore Structure Analysis

The various theories for the surface area and pore structure are discussed as follows.

4.7.1 Determination of the Total Pore Volume

The total pore volume is obtained from the adsorption amount near $P/P_0 = 1$, by assuming that the pores are filled with liquid adsorbate at the measurement temperature.

In the case of N_2 adsorption at 77 K, the N_2 liquid density at 77 K is 0.808 g mL^{-1}. If the adsorption isotherm has flat region near P/P_0, which has only micropores, the pore volume is well defined. However, the material has macropores the isotherm raises rapidly near P/P_0 = 1 and the limit of large macropores may exhibit an essentially vertical rise. When there is the standard material which has no nanopores such as carbon black, the accurate pore volume is obtained from the α_s analysis [5].

4.7.2 Langmuir Equation [20]

Type I isotherm, fitted for the chemical adsorption isotherm and the physical adsorption isotherm having micorpores, is expressed Langmuir equation. The Langmuir equation derived from the kinetic theory is expressed as

$$n = \frac{abP}{1 + aP} \qquad (4.7.2.1)$$

where *a* is the adsorption coefficient related to an equilibrium constant and *b* is the saturation adsorption amount. Langumir assumed that the energy of adsorption for the first layer is generally considerably larger than for the second and higher layers and therefore multilayer formation do not occur. The saturation adsorption amount b is equal to the monolayer capacity. The equation (4.7.2.1) is converted to

$$P / n = 1 / ab + P / b \qquad (4.7.2.2)$$

If the plot of P vs P/n has a linearity, a and b are obtained from the slope and intercept of the plot.

4.7.3 BET Equation [21]

The Brunauer-Emmett-Teller (BET) method is the most used for the determination of the surface area of the solid material. The BET theory is based on the Langmuir kinetic

theory. Although the Langmuir theory assumes that the adsorption occur only monolayer, the BET theory assumes that the adsorption occurs multilayer on the surface. The BET theory also assumes that the first adsorption layer interacts with solid surface and the adsorbed molecules of higher layer interact with only the adsorbed molecules. The BET equation is expressed as

$$\frac{n}{n_m} = \frac{Cx}{(1-x)(1-x+Cx)} \qquad (4.7.3.1)$$

Here, n_m is the monolayer capacity, C is the constant value related to the energy of adsorption in the first adsorbed layer, and x is the relative pressure (P/P_0). The equation (4.7.3.1) can change to (4.7.3.2)

$$\frac{x}{n(1-x)} = \frac{C-1}{n_m C}x + \frac{1}{n_m C} \qquad (4.7.3.2)$$

The BET equation requires a linear plot of x/n(1-x) vs x in the relative pressure range of 0.05 to 0.30. This linear region is shifted to lower relative pressure of 0.01 to 0.10 for micropores materials [22]. The n_m and C are obtained from the slope and intercept of the plot. The specific surface area, S, can be determined from n_m value. The specific surface area is calculated by next equation.

$$S = \frac{n_m N a_m}{1000 M} \quad (m^2/g) \qquad (4.7.3.3)$$

Here, the unit of n_m is mg/g, N is the Avogadro constant, M is the molecular weight of adsrbate, and a_m is the average area occupied by a molecule of adsorbate. a_m is 0.162 nm^2 for N_2 adsorption at 77 K. In other gases, a_m is obtained from the literature [5,23-25]. Although the n_m value is also obtained from the Langumir equation, this n_m is not applicable to porous material containing both micropores and meso and/or macropores.

4.7.4 Dubinin-Radushkevich (DR) equation [26,27]

The DR equation is based on the Polanyi potential theory of adsorption as expressed by

$$\frac{W}{W_0} = exp\left[-\frac{A}{\beta E_0}\right] \qquad (4.7.4.1)$$

where, W and W_0 is an adsorption amount at P/P_0 and saturated adsorption amount, respectively, β is an affinity coefficient which is the constant value for each gas, E_0 is a characteristic adsorption energy, and A is the Polanyi potential [28] expressed as

$$A = -RT\,ln(P_0 / P) \qquad (4.7.4.2)$$

Equation (4.7.4.2) is converted to transform Equation (4.7.4.3)

$$lnW = -\left(\frac{RT}{\beta E_0}\right)^2 ln^2\left(\frac{P_0}{P}\right) + lnW_0 \qquad (4.7.4.3)$$

A linear relationship should be obtained between lnW and $ln^2(P_0/P)$. W_0 and E_0 can be obtained from the slope and intercept of the DR plot. A micropore volume can be determined by W_0 using liquid density at the measurement temperature.

References

(1) F. Rouquerol, J. Rouquerol, and K. Sing, “Adsorption by Powder & Porous Solids: Principles, Methodology and Applications” Academic Press, San Diego, 1999.

(2] K. Kaneko, “Coroido Kagaku I. Chapter 11” Tokyo Kagaku Douzin, Tokyo, 1995.

(3) W. A. Steele, *Surf. Sci.* **36**, 317 (1973).

(4) K. S. W. Sing, D. H. Everett, R. A. W. Haul, L. Mosccou, R. A. Pierotti, J. Rouquerol, T. Siemieniewska, *Pure Appl. Chem.* **57**, 603 (1985).

(5) S. J. Gregg, K.S.W. Sing, “Adsorption, Surface Area and Porosity” Academic Press, New York, 1982.

(6) S. Brunauer, L. S. Deming, W. S. Deming, and E. Teller, *J. Am. Chem. Soc.* **62**, 1723 (1940).

(7) K. S. W. Sing, “ Porosity in Carbon” Edward Arnold, London, 1995.

(8) K. Murata and K. Kaneko, *Chem. Phys. Lett.* **321**, 342 (2000).

(9) J. W. Gibbs, “Collected Works”, Longmans Green and Co., New York, 1877.

(10) P. H. Emmett and S. Brunauer, *J. Am. Chem. Soc.* **56**, 35 (1937).

(11) P. H. Emmett, *Adv. Colloid Sci.* **48**, 690 (1926).

(12) J. W. McBain, and A. M. Bakr, *J. Am. Chem. Soc.* **48**, 690 (1926).

(13) K. Kaneko, K. Shimizu, T. Suzuki, *J. Chem. Phys.* **97**, 8705 (1992).

(14) G. H. Findenegg, B. Korner, J. Fischer, M. Bohn, *Ger. Chem. Eng.* **6**, 80 (1983).

(15) R. K. Agarwal, J. A. Schwarz, *Carbon* **26**, 873 (1988).

(16) O. Talu, S. –Y. Zhang, D. T. Hayhurst, *J. Chem. Phys.* **97**, 12894 (1993).

(17) P. Malbrunot, D. Vidal, J. Vermesse, R. Chahine, and T. K. Bose, *Langmuir*, **8**, 577 (1992).

(18)P. Malbrunot, D. Vidal, J. Vermesse, R. Chahine, and T. K. Bose, *Langmuir*, **13**, 539 (1997).

(19) M. Ruike, T. Kasu, N. Setoyama, T. Suzuki, and K. Kaneko, *J. Phys. Chem.* **98**, 9594 (1004).

(20) I. Langmuir, *J. Am. Chem. Soc.* **40**, 1361 (1918).

(21) S. Brunauer, P. H. Emmett, E, Teller, *J. Am. Chem. Soc.* **60**, 309 (1938).

(22) K. Kaneko, R. F. Cracknell, D. Nicholson, *Langmuir*, **10**, 4606 (1994).

(23) W. A. Steele, *J. Chem. Phys.* **25**, 819 (1956).

(24) A. L. McClellan, H. F. Harnsberger, *J. Colloid Interface Sci.* **23**, 577 (1967).

(25) I. M. K. Ismail, *Carbon*, **28**, 423 (1990).

(26) M. M. Dubinin, *Chem. Rev.* **60**, 235 (1960).

(27) M. M. Dubinin, L. V. Radushkevich, *Proc. Acad. Sci.* USSR **55**, 331 (1947).

(28) M. Polanyi, *Verb. Deutsch Phys.* **16**, 1012 (1914). (2005)

5. Gas Adsorptivities of Pitch-based ACF

5-1 Introduction

The characteristics of gas adsorption depend on difference in adsorbates. In this chapter, I show the results of adsorption experiments about toluene, hydrogen, and deuterium. Toluene is organic vapor, and used for the equilibrium adsorption measurement of the adsorbent as an example of the aromatic hydrocarbon-based solvent.

It is effective for the comparative examination with various organic solvents and comparison of the adsorbents properties.

5-2 Toluene adsorption properties

5-2-1 Introduction

First, I show the characteristic based on the toluene adsorption.

5-2-2 Experimental

The experiment carried out in conformity to the test methods for fibrous activated carbon, JIS K 1477, 6.8 toluene adsorptivity.

5-2-3 Results and Discussion

Fig.5-2-1 shows adsorption isotherm of toluene as a typical example of the gas phase adsorption. For the gas phase adsorption, an adsorbed amount was proportional to a specific surface area, because of adsorption on micropores.

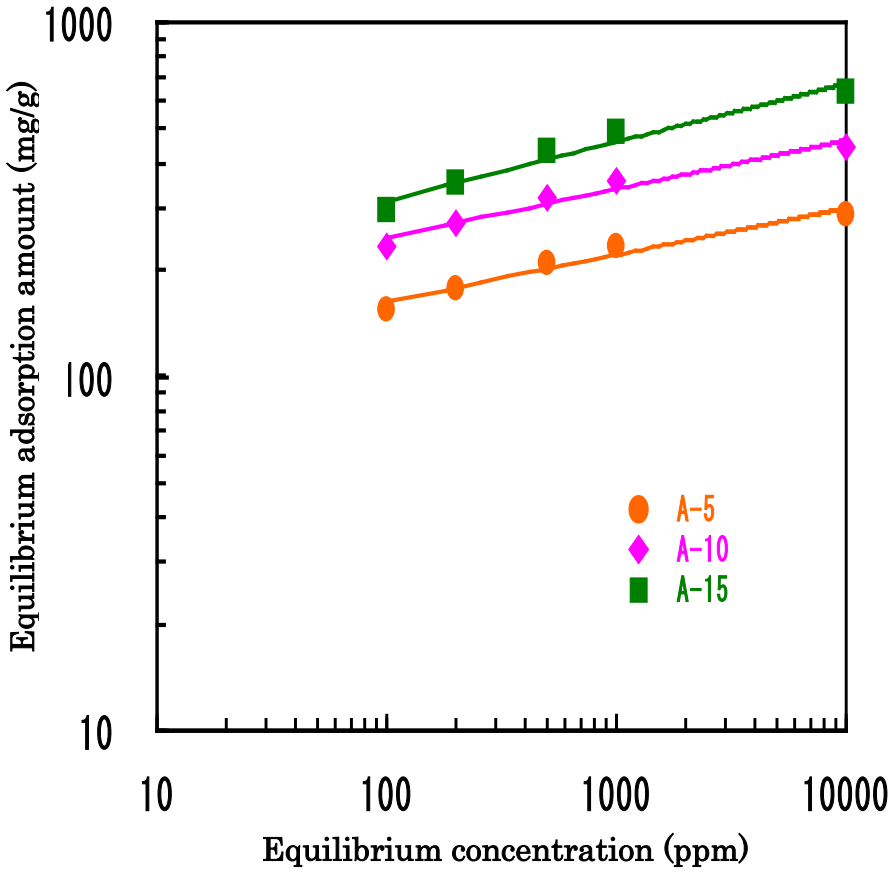

Fig. 5-2-1 Adsorption isotherm of toluene on ACFs

5-3 Quantum Sieving Effect of Modified Activated Carbon Fibers on H_2 and D_2 Adsorption at 20 K

5-3-1 Abstract

Quantum sieving of activated carbon fibers (ACFs) and their fluorides was observed for H_2 and D_2 adsorption at 20 K. Fluorination reduced the slit-shaped pore width of ACFs by 0.2 nm. The activated carbon fibers can act as highly efficient quantum sieves for H_2 and D_2, because the effective size of an H_2 molecule is larger than that of a D_2 molecule due to the uncertainty principle and the molecular size difference between H_2 and D_2 is significant in the micropore space. The D_2/H_2 selectivity of ACFs evaluated by ideal adsorption solution theory was larger than that of the fluorinated ACFs.

5-3-2 Introduction

Molecular sieving materials of high performance have been becoming important in the variety of areas such as adsorption and catalysis for environmentally friendly techniques.[1-3] The classical molecular sieving process is based on the difference of the penetration ability in the pores that depends on the classical molecular size. This classical sieving principle of the molecular size cannot be applied to isotope separation, because the isotopic molecules have identical molecular quantities except for the atomic mass. In contrast to classical molecular sieving a quantum molecular sieving process applicable to the isotope separation was proposed by Beenakker and co-workers.[4] Quantum molecular sieving is based on the preferential adsorption of heavier isotopes due to the difference in the quantum mechanical energy levels of atoms or molecules confined in the very narrow space that is comparable to the de Broglie thermal

wavelength. Johnson and co-workers developed the quantum molecular sieving concept for the separation of isotopes of H_2 and other molecules in single wall carbon nanotubes and zeolites by computer simulation.[5-7] They indicated that the heavier molecules such as T_2 will be adsorbed in micopores that exclude lighter molecules such as H_2 through the quantum sieving effect by using the realistic model and path integral calculations. Some theoretical works have been done to examine the effect of the potential on quantum sieving selectivities in nanopores.[8-12] Recently, Tanaka et al. showed experimentally the significant quantum molecular sieving effect of single wall carbon nanohorns (SWNHs) against H_2 and D_2 with the support of grand canonical Monte Carlo simulation with the aid of Feynman-Hibbs approximation.[13-15] The quantum molecular sieving for H_2 and D_2 is quite valuable in materials and energy technologies. An application of popular porous materials to the quantum molecular sieving for H_2 and D_2 is of great significance. Quantum sieving can be observed with both cylindrical pores and slit pores, where the quantum confinement of adsorbate is two-dimensional and one-dimensional, respectively. In the slit pores, molecules adsorb near the pore walls, leading to the 1D type of quantum confinement. When the pore diameter is almost the same as that of molecules, the adsorbed molecules are highly confined in cylindrical pores due to the 2D type of quantum confinement. In this work, we present the quantum molecular sieving effect of H_2 and D_2 in activated carbon fibers(ACFs) and their fluorides (F-ACFs). The ACFs are commercially available adsorbents of high microporosity and good model systems for the 1D type of quantum confinement. The ACFs have considerable homogeneous slit-shaped micropores that consist of micrographites. The basal plane of micrographites is very inert and does not react with most chemical species except for oxygen and fluorine. The ACFs readily react with

elemental fluorine in the temperature range of room temperature to 415 K to form fluorinated ACFs (F-ACFs).[16,17] Kaneko and co-workers have reported the adsorption properties of F-ACFs in detail and have shown that the fluorination of ACFs led to a decrease in the pore width.[18-21] The narrowing of the pore width should be effective on the quantum sieving because the transverse motion of molecules must be quantized.4 In this section, we focused on the marked adsorption difference for H_2 and D_2 on ACFs and F-ACFs at 20 K, which can be ascribed to the quantum sieving selectivity.

5-3-3 Experimental Section

Pitch-based activated carbon fibers (A20, AD'ALL Co., Ltd.) were used for fluorination. The ACFs were heat-treated at 573K in vacuo prior to fluorination. Fluorined ACFs were prepared by direct reaction of ACFs with elemental fluorine (purity99.7%, Daikin Industries, Ltd.). The reaction was run for 24 h at 373 K with 0.1 MPa of fluorine gas. X-ray photoelectron spectroscopy (XPS) measurements were carried out using a Shimadzu ESCA850 instrument with Mg KR (1253.6 eV) X-rays for the ionizing radiation provided by an X-ray source working at 240 W. The adsorption isotherms for N2 were measured by means of an automatic volumetric sorption analyzer (Autosorb-1, Quantaqurome) at 77 K. The adsorption isotherms for H_2 and D_2 were measured at 20 K by means of the volumetric apparatus composed of cryostat with a He closed cycle refrigerator.[13-15]

5-3-4 Results and Discussion

The fluorinated ACFs (F-ACFs) were obtained by thermal fluorination at 373 K. The composition (F/C) determined by gravimetry was 0.58. Fig. 5-3-1 shows the C 1s and F

1s XPS spectra obtained on the surfaces of the F-ACFs. The C 1s XPS spectrum of F-ACF has four peaks at 290.6, 289.0, 286.8, and 284.5 eV. These peaks are assigned to CF_2 groups, C-F bonds, C atoms whose nearest neighbors have a C-F bond, and sp^2 C atoms, respectively. The F 1s spectrum showed a main peak at688.0 eV and a small shoulder at 685.1 eV. The XPS results clearly showed that the ACFs can react with fluorine to form their fluorides. In the fluorination of the ACFs, the C-F bondsare formed on their pore walls. Although each layer of micrographite is buckled, the layered structure is preserved after the fluorination.

Fig. 5-3-2 shows the N_2 adsorption isotherms on ACFs and F-ACFs at 77 K. Both isotherms are of type I, suggesting that both samples are highly microporous. The decrease in the amount of N_2 adsorbed on the F-ACFs is observed due to the narrowing of the micropores and the weight increase of the pore walls by fluorination. The α_S plots of ACFs and F-ACFs were obtained using the reference data of carbon black and fluorinated carbon black, respectively. The αs plot of ACFs shows two upward deviations from linearity below $\alpha_s = 1.0$. The upward deviation in a low αs region originates from the monolayer adsorption enhanced by the micropore field (filling swing), while another upward deviation in the α_s range from 0.7 to 1.0 is due to the filling of molecules in the residual space between the monolayers on both pore walls (cooperative swing). The α_s plot of F-ACFs had a single filling swing, indicating a significant reduction of the micropore width; the cooperative swing is not observed due to the narrow space on the monolayer-formed pore to accept another layer. The average micropore width of F-ACFs can be evaluated from their α_s plot, assuming the micropores of F-ACFs retain their slit-shaped geometry. The micropore width and other pore parameters calculated from the α_s plots of ACFs and F-ACFs were tabulated in

Table 5-3-1. The average micropore widths of ACFs and F-ACFs were calculated as 1.09 and 0.88 nm, respectively, indicating the decrease in the micropore width by the fluorination. The decrease in the micropore width by fluorination can be described as the change in the pore walls from the graphene layers to the fluorinated layers. The N_2 adsorption isotherms were analyzed by the Dubinin-Radushkevich (DR) equation, which gives the micropore volume, W_0, and the characteristic adsorption energy, βE_0. Here, β is an affinity constant. βE_0 gives rise to the isosteric heat of adsorption at the fractional filling of e^{-1}, $\Delta H_{\mathrm{iso},1/e}$. The W_0 and $\Delta H_{\mathrm{iso},1/e}$ values of ACFs and F-ACFs are also shown in Table 5-3-1. The W_0 value of the ACFs remarkably decreases by fluorination, suggesting a weight increase of the pore wall by fluorination and narrowing of the pore width by the formation of C-F bonds on the pore walls. The $\Delta H_{\mathrm{iso},1/e}$ value of the F-ACFs was much smaller than that of the ACFs, indicating the formation of a lower energy surface by fluorination. These results suggest that the micrographitic pore walls of ACFs are converted into the walls coated with covalent C-F bonds by the fluorination.

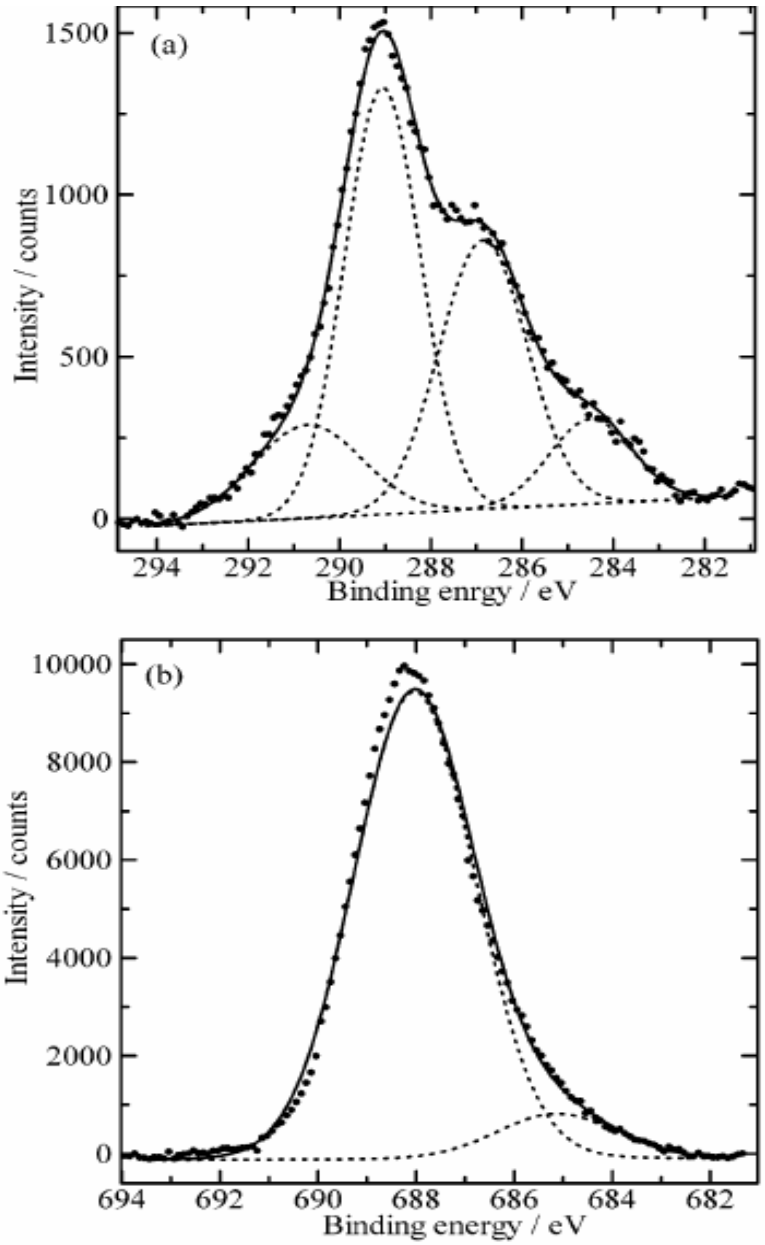

Fig. 5-3-1 (a) C 1s and (b) F 1s XPS spectra obtained on the surfaces of the F-ACFs.

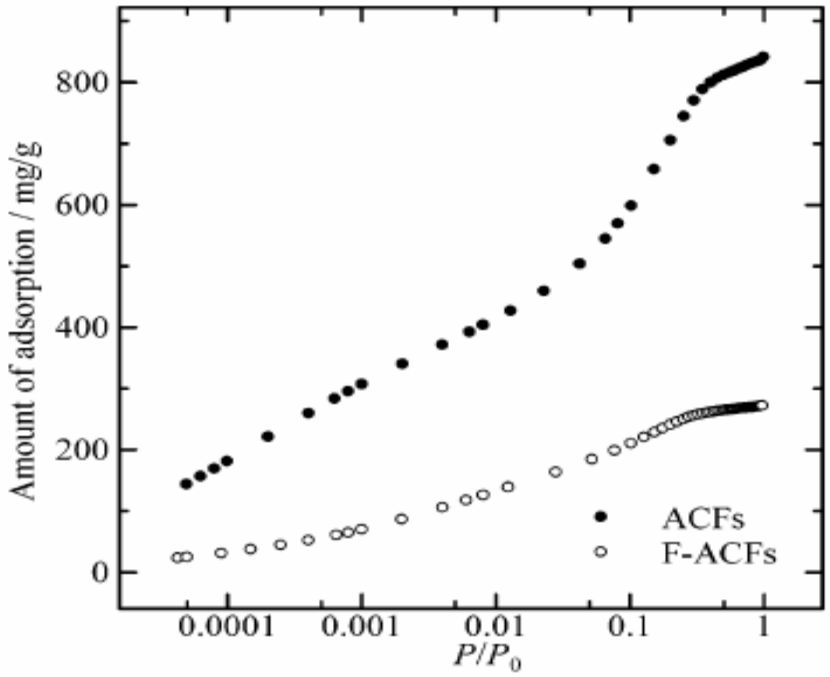

Fig. 5-3-2 Nitrogen adsorption isotherms of ACFs (closed circles) and F-ACFs (open circles) at 77 K.

Table 5-3-1 **Pore Structural Parameters of ACFs and F-ACFs Calculated from N_2 and H_2 Adsorption Isotherms at 77 and 20 K, Respectively**[a]

	a_{total} (m^2/g)	a_{ext} (m^2/g)	w (nm)	W_0 (cm^3/g)	$\Delta H_{iso,1/e}$ (kJ/mol)	S_{BET} (m^2/g)
Nitrogen Adsorption Isotherms at 77 K						
ACF	1675	37	1.1	0.59	11.7	1670
F-ACF	740	18	0.9	0.24	10.0	670
Hydrogen Adsorption Isotherms at 20 K						
ACF				0.62	3.6	1850
F-ACF				0.30	3.2	830

[a] a_{total}, a_{ext}, and w are the total surface area, external surface area, and pore width calculated from α_s analysis, respectively. W_0 and $\Delta H_{iso,1/e}$ are the micropore volume and isosteric heat of adsorption at the fractional filling of e^{-1} calculated from the DR equation, respectively. S_{BET} is the surface area calculated from BET theory.

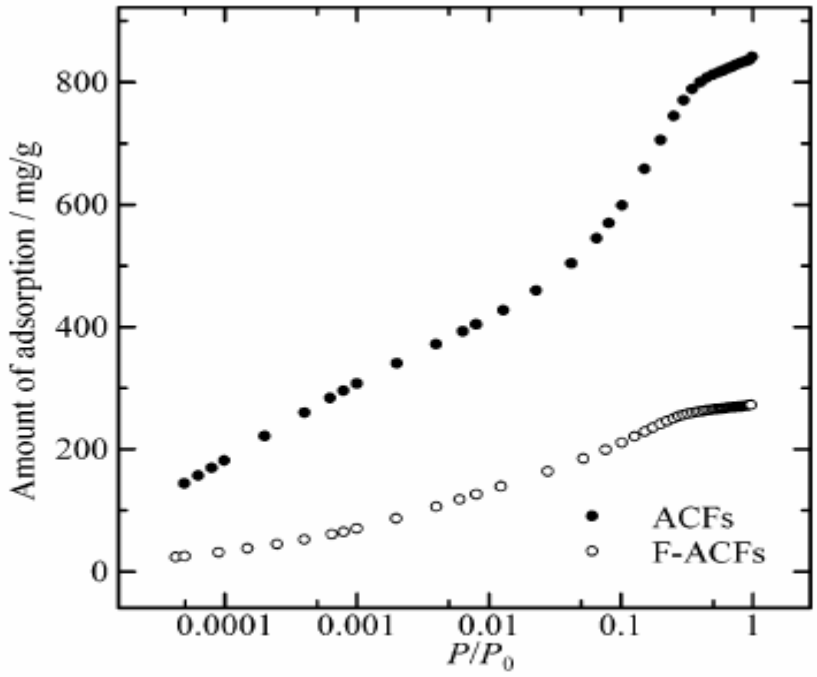

Fig. 5-3-3 Hydrogen adsorption isotherms of ACFs (closed circles) and F-ACFs (open circles) at 20 K.

Fig. 5-3-3 shows the H_2 adsorption isotherms of ACFs and F-ACFs at 20 K. The isotherms for both samples were of type I, indicating the strongly enhanced filling for H_2 vapors similarly to N_2. The H_2 adsorption isotherms of ACFs and F-ACFs were analyzed with Brunauer-Emmett-Teller (BET) and DR plots.The BET surface area and micropore volume evaluated from the H_2 adsorption isotherms are larger than those obtained from the N_2 adsorption isotherms, owing to the differences in the sizes of the probe molecules.

Fig. 5-3-4 shows the adsorption isotherms of H_2 and D_2 at 20K for (a) ACFs and (b) F-ACFs. The adsorption amount of D_2 is explicitly larger than that of H_2 for ACFs and F-ACFs except for adsorption on F-ACFs below 2×10^{-4} of $P/P0$, as shown in Fig. 5-3-4. This remarkable adsorption difference should come from the quantum sieving effect. The zero-point energy difference of molecules in micropores can be attributed to the differences in the mass of the molecules, *m*, and pore widths, *w*; that is, the

difference in the energy levels of isotopic molecules increases with a decrease of *m* and *w*, inducing themarked quantum effect.

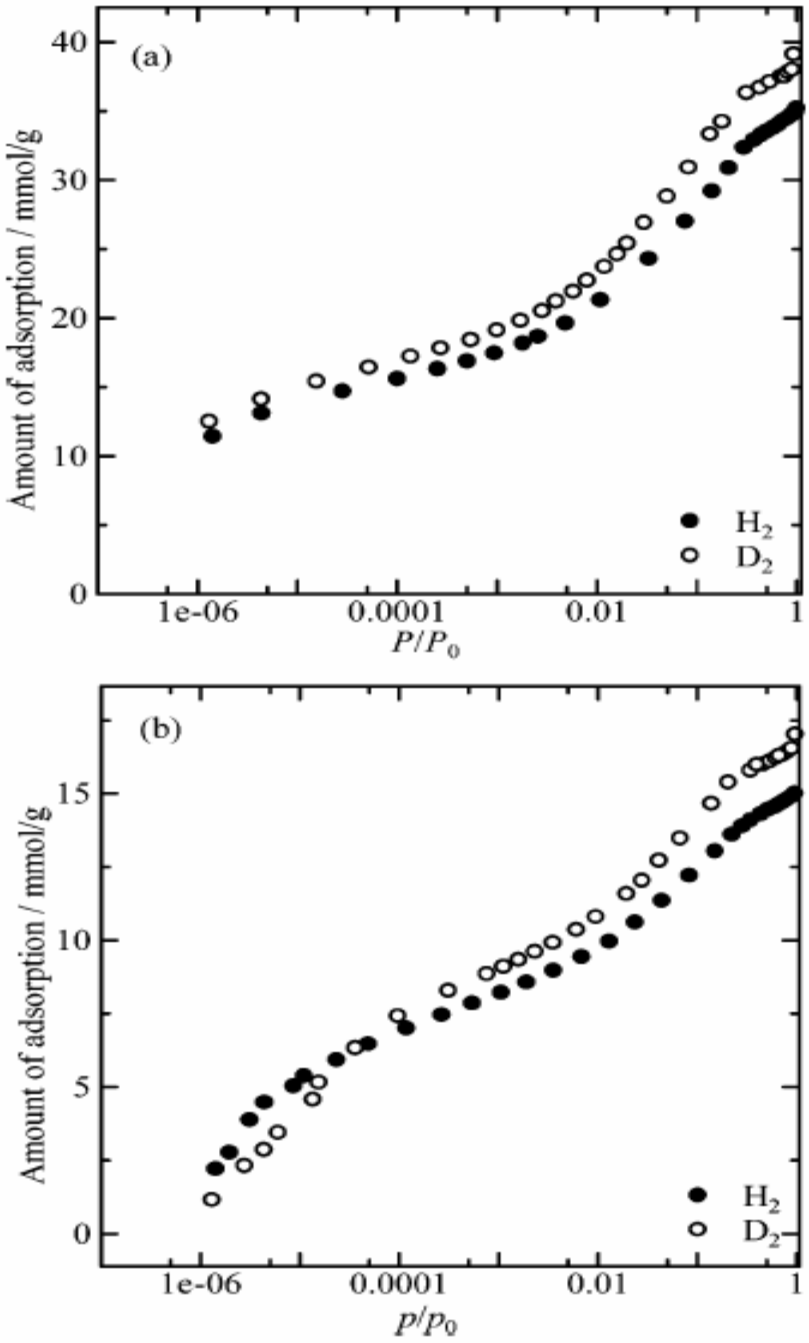

Fig. 5-3-4 Adsorption isotherms of H_2 (closed circles) and D_2 (open circles) at 20 K for (a) ACFs and (b) F-ACFs.

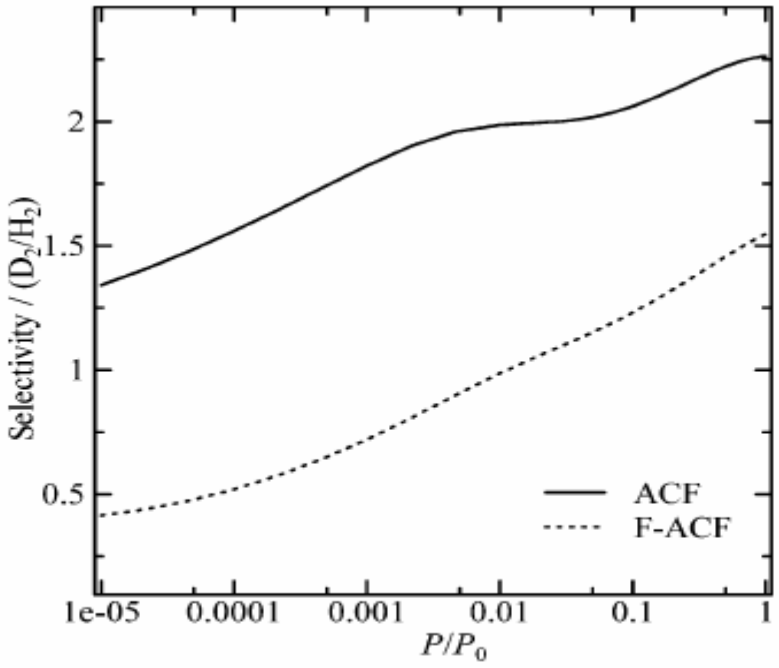

Fig. 5-3-5 Selectivity in the slitlike pores of ACFs and F-ACFs at 20 K for D_2 over H_2 calculated by IAST.

The H_2 and D_2 adsorption isotherms are used to predict the selectivities of H_2 and D_2 based on ideal adsorption solution theory (IAST).[22] The pure fluid isotherms for each H_2 and D_2 have been fitted by multiple Langmuir equations to apply IAST. The selectivities based on IAST are calculated over a range of pressures and are shown in Fig. 5-3-5. The D_2/H_2 selectivites of ACFs and F-ACFs increase with the relative pressure. The selectivity of ACFs is larger than unity over the whole P/P_0 range, whereas the selectivity of F-ACFs becomes larger than unity above P/P_0) 10^{-2}. In the case of the quantum molecular sieving effect, H_2 molecules occupy more volume than D_2 molecules in the pore space and thereby the selectivity of D_2/H_2 should be larger than unity, as observed in ACFs. This selectivity due to the quantum molecular sieving effect is based on the equilibrium adsorption. Recently, Kumar and Bhatia reported a

molecular dynamics simulation on quantum molecular sieving for adsorption kinetics in nanopores at 50 K, showing that the heavier D_2 molecules diffuse faster than the lighter H_2 molecules below 150 K.[23] If the adsorption in F-ACFs is not in equilibrium due to the narrower pores, the adsorption behavior should be governed by the adsorption kinetics; the D_2/H_2 kinetic selectivity of F-ACF must go over unity. The observed result for F-ACFs at 20 K is far below the predictions by equilibrium and kinetic quantum molecular sieving effects. The micropore wall structures of F-ACF are completely different from those of ACFs. The pore walls of F-ACF have saw-shaped structures in the sub-nanoscale, being different from graphene wall structures of ACFs. These unique saw-shaped wall structures should intervene in the diffusion of heavier D_2 molecules, reducing the D_2/H_2 selectivity value. Accordingly, there is a great possibility that sub-nanoscale wall roughness of the small micropores gives rise to an essential effect on the quantum molecular sieving.

References

(1) Go¨ltner, C. G.; Smarsly, B.; Berton, B.; Antonietti, M. *Chem. Mater*. **2001**, *13*, 1617.

(2) Sakthivel, A.; Huang, S.; Chen, W.; Lan, Z.; Chen, K.; Kim, T.;Ryoo, R.; Chiang, A. S. T.; Liu, S. *Chem. Mater*. **2004**, *16*, 3168.

(3) Yuan, W.; Lin, Y. S.; Yang, W. *J. Am. Chem. Soc.* **2004**, *126*,4776.

(4) Beenakker, J. J. M.; Borman, V. D.; Krylov, S. Y. *Chem. Phys. Lett*. **1995**, *232*, 379.

(5) Wang, Q.; Challa, S. R.; Sholl, D. S.; Johnson, J. K. *Phys. Re*V. *Lett*. **1999**, *82*, 956.

(6) Challa, S. R. Sholl, D. S.; Johnson, J. K. *Phys. Re*V. *B* **2001**, *63*, 245419.

(7) Challa, S. R. Sholl, D. S.; Johnson, J. K. *J. Chem. Phys*. **2002**, *116*, 814.

(8) Gordillo, M. C.; Boronat, J.; Casulleras, J. *Phys. Re*V. *B* **2001**, *65*, 14503.

(9) Hathorn, B. C.; Sumpter, B. G.; Noid, D. W. *Phys. Re*V. *A* **2001**, *64*, 22903.

(10) Lu, T.; Gold field, E. M.; Gray, S. K. *J. Phys. Chem. B* **2003**, *107*, 12989.

(11) Garberoglio, G.; DeKlavon, M. M.; Johnson, J. K. *J. Phys. Chem. B* **2006**, *110*, 1733.

(12) Lu, T.; Goldfield, M.; Gray, S. K. *J. Phys. Chem. B* **2006**, *110*, 1742.

(13) Tanaka, H.; Kanoh, H.; Mustapha, E.; Steele, W. A.; Yudasaka, M.; Iijima, S.; Kaneko, K. *J. Phys. Chem*. **2004**, *108*, 17457.

(14) Tanaka, H.; Fan, J.; Kanoh, H.; Yudasaka, M.; Iijima, S.; Kaneko, K. *Mol. Simul*. **2005**, *31*, 465.

(15) Tanaka, H.; Kanoh, H.; Yudasaka, M.; Iijima, S.; Kaneko, K. *J. Am. Chem. Soc*. **2005**, *127*, 7511.

(16) Touhara, H.; Okino, F. *Carbon* **2000**, *38*, 241.

(17) Touhara, H.; Inahara, J.; Mizuno, T.; Yokoyama, Y.; Okamoto, S.; Yanagiuchi, K.; Mukopandhyay, I.; Kawasaki, S.; Okino, F.; Shirai, H.; Xu, W. H.; Kyotani, T.; Tomita, A. *J. Fluorine Chem*. **2002**, *114*, 181.

(18) Li, G.; Kaneko, K.; Ozeki, S.; Okino, F.; Ishikawa, R.; Kanda, M.; Touhara, H. *Langmuir* **1995**, *11*, 716.

(19) Li, G.; Kaneko, K.; Okino, F.; Ishikawa, R.; Kanda, M.; Touhara, H. *J. Colloid Interface Sci*. **1995**, *172*, 539.

(20) Setoyama, N.; Li, G.; Kaneko, K.; Okino, F.; Ishikawa, R.; Kanda, M.; Touhara, H. *Adsorption* **1996**, *2*, 293.

(21) Kaneko, K.; Setoyama, N.; Li, G.; Okino, F.; Ishikawa, T.; Kanda,M.; Touhara, H. *TANSO* **1999**, *187*, 71.

(22) Myers, J. J.; Prausnitz, V. D. *AIChE J*. **1965**, *11*, 121.

(23) Kumar, A. V.; Bhatia, S. K. *Phys. Re*V. *Lett*. **2005**, *95*, 245901.

5-4 Defluorination-enhanced hydrogen adsorptivity of activated carbon fibers

5-4-1 Abstract

Fluorinated activated carbon fibers (F-ACFs) were prepared by direct thermal fluorination of pristine activated carbon fibers. By the pyrolysis of F-ACFs at 1073 K under nitrogen gas flow, fluorine was subsequently eliminated and the sp^2-bonded ACF structures were recovered. The micropore widths were 1.1 and 0.8 nm, and the isosteric heats of adsorption of nitrogen were 11.3 and 12.8 kJ/mol for pristine and defluorinated ACFs, respectively. These results strongly suggest that changes occurred in the structural properties of micropores in defluorinated ACFs. The hydrogen adsorption isotherms showed that the defluorinated ACFs adsorbed more hydrogen gas than pristine ACFs at 77 K, suggesting that the potential for interaction between hydrogen molecules and the defluorinated slit nanospaces was increased due to the changes in the pore structural properties and/or to the induced polarization of the pore walls making up the modified p-electron systems.

5-4-2 Introduction

Considerable interest has been generated in the application of hydrogen, a perfect energy carrier, as a clean fuel for automobiles or fuel cells, thus stimulating new intensive development of efficient hydrogen storage and transportation media. Adsorption of hydrogen molecules on carbon materials is being considered as one of the solutions for hydrogen storage. The candidates for hydrogen storage media are activated carbons, carbon nanotubes, metal organic frameworks, and so on,[1-7)] but no existing

adsorbents fully satisfy the target values yet. Therefore, it is crucial to elucidate key structural factors for hydrogen adsorptivity in order to design better carbon adsorbents and hence, well-characterized porous carbons must be used for the study on the relationship between hydrogen adsorption and structural factors. Activated carbon fibers (ACFs) consist of micrographite units which enclose mono-dispersed micropores, and their physical properties and nanostructures have been proactively studied for more than 15 years by Kaneko et al.[8–17] Hence, the ACFs are good model systems for chemical modification in the search for key factors for hydrogen adsorption. Ordinarily, various chemical modifications have been applied to donate specific affinities to target molecules or media. Among them, fluorination is a powerful method to introduce hydrophobicity. At the same time, fluorination modifies the nanostructures and physical properties of carbon materials.[18,19] In particular, Kaneko et al. have reported that the adsorptive properties of ACFs are effectively modified by fluorination.[20–23] As fluorination changes dramatically the carbon bonding state from sp^2 to sp^3, controlled fluorination can alter electronic and pore structures of ACFs according to desired designs.

The fluorine can be eliminated by pyrolyzing the fluorinated carbons in inert gas or in a vacuum, and the π-electron systems can be largely recovered by pyrolysis.[24–27] Defluorination is expected to increase the number of defective sites, because fluorinated regions become etched during defluorination. Accordingly, defluorination of the fluorinated ACFs can introduce structural changes and lattice imperfections in their pore walls. The changes in the structural and electronic properties induced by defluorination are expected to improve the hydrogen adsorptive properties of ACFs, because the defects have increased interaction potential for interaction with hydrogen while the

metastable electronic structure between sp^2 and sp^3 bonding states can have a larger polarization effect on hydrogen adsorption.

In this section, we prepared fluorinated ACFs (F-ACFs) by direct thermal fluorination and, subsequently, defluorinated ACFs by the pyrolysis of the F-ACFs. The structural properties of the defluorinated ACFs were characterized by means of X-ray photoelectron spectroscopy (XPS), X-ray diffraction (XRD), Raman spectroscopy, and nitrogen adsorption isotherms at 77 K. The hydrogen adsorptive properties of defluorinated ACFs were studied by means of hydrogen adsorption isotherms at 77 K.

5-4-3 Experimental

Pitch-based ACFs (A20, AD'ALL Co. Ltd.) were used for fluorination. Fluorinated ACFs were prepared by directly reacting ACFs with elemental fluorine gas (Daikin Industries, Ltd.) at 373 K for 24 h. The ACFs were later defluorinated by the pyrolysis of the F-ACFs at 1073 K under nitrogen gas flow. XPS measurements were carried out using a JEOL JPS-9010MX with Mg K_α X-rays. XRD measurements were carried out using a powder X-ray diffractometer (Miniflex, Rigaku) with Cu K_α radiation.Raman spectra (NRS-1000, JASCO) were measured at room temperature using the 532 nm line of a YAG laser. Pore structures were characterized based on nitrogen adsorption isotherms at 77 K. The micropore widths of pristine and defluorinated ACFs were calculated by αs-plots. The αs-plots of pristine and defluorinated ACFs were obtained using the reference data of nonporous carbon black. The nitrogen adsorption isotherms of pristine and defluorinated ACFs were analyzed by the Dubinin–Radushkevich (DR) equation, which gives the micropore volume W_0 and the characteristic adsorption energy βE_0. Here b is an affinity constant. The βE_0 gives the isosteric heat of adsorption

at the fractional filling of e^{-1}, $\Delta H_{iso,1/e}$. The adsorption isotherms for hydrogen were measured by means of a volumetric adsorption apparatus (Autosorb-1, Quantachrome) at 77 K.

5-4-4 Results and discussion

Fig. 5-4-1 shows the C 1s and F 1s XPS spectra of pristine, fluorinated, and defluorinated ACFs. The spectrum of pristine ACFs shows a peak centred at 284.5 eV and broad shoulder peaks at 286-288 eV. The former is due to the C–C bonded carbon atoms with sp^2 configurations and the latter to the carbon atoms bonded to oxygen atoms. In addition to these peaks, the C 1s spectrum of F-ACFs exhibits peaks originating from CF (291 eV) and CF_2 (293 eV) groups on the higher binding energy side. The F1s spectrum of F-ACFs is also clearly observed at 690 eV. This binding energy value is close to that of the C-F covalent bond. The XPS spectra of F-ACFs indicate that the C-F bonds, which are similar to those of the graphite fluorides, are formed on the surface of F-ACFs. After pyrolysis, the C 1s XPS spectrum showed that a series of peaks assigned to fluorine functional groups almost com-pletely disappeared. Also, the F 1s XPS spectrum of deflurinated ACFs showed a barely discernible peak in the F 1s region. These results suggest that the fluorine atoms are eliminated and the sp^2 electron systems are almost fully recovered by the pyrolysis.

Fig. 5-4-2 shows the XRD patterns of pristine, fluorinated, and defluorinated ACFs. The intense small angle scattering observed for all the samples is due to the presence of micropores. The XRD profile of F-ACFs shows broad diffraction peaks at 12° and 41° corresponding to (002) and (100) reflections of graphite fluorides, respectively. The small angle scattering for F-ACFs becomes weaker than that for ACFs, indicating the

lesser contribution by F-ACFs micropores. Defective graphitic units on ACFs are most likely decomposed to low molecular weight fluorocarbons upon fluorination.

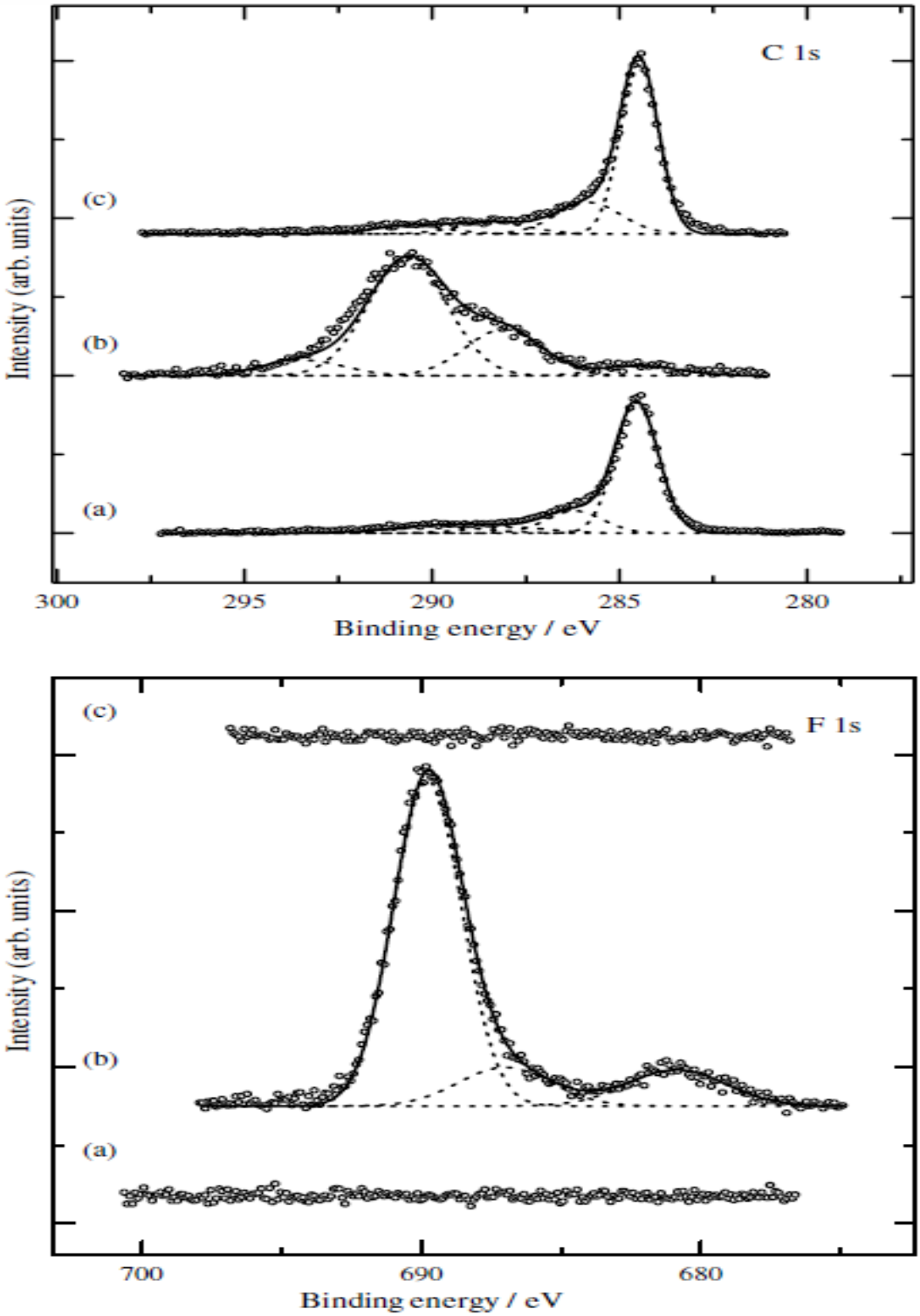

Fig. 1. C 1s and F 1s XPS spectra of (a) pristine activated carbon fibers, (b) fluorinated ACFs and (c) defluorinated ACFs.

Fig. 5-4-1

The XRD pattern of defluorinated ACFs showed the recovery of their original state

following desorption of their fluorine. However, a slight shift of the d_{002} value from 0.37 nm to 0.36 nm was observed, suggesting some contraction of the interlayer spaces in the micrographite. Also the defluorination lowers the small angle X-ray scattering. Although the fluorinated regions are likely etched or damaged by pyrolysis, we can conclude that a majority of the micropore structures has been recovered.

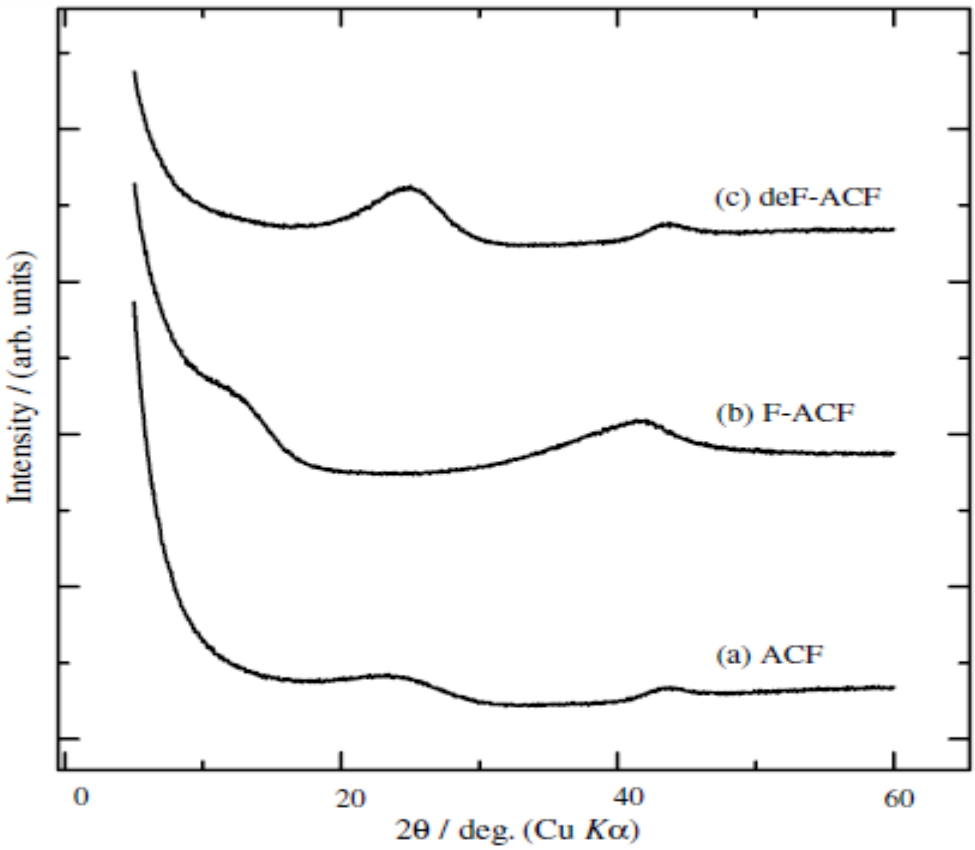

Fig. 5-4-2 XRD patterns of (a) pristine activated carbon fibers, (b) fluorinated ACFs and (c) defluorinated ACFs.

Fig. 5-4-3 shows Raman spectra of ACFs and defluorinated ACFs. Two Raman bands are observed around 1340 and 1600 cm^{-1}, where these bands are characteristic of disordered and ordered graphitic sp^2 carbons and are thus designated as D and G bands, respectively. The spectra of defluorinated ACFs show similarities to those obtained

from the pristine sample, but the D band intensities increased slightly after defluorination. The Raman data indicated that the defluorinated ACFs recovered their disordered sp^2-carbon structures and became slightly more defective than the starting materials.

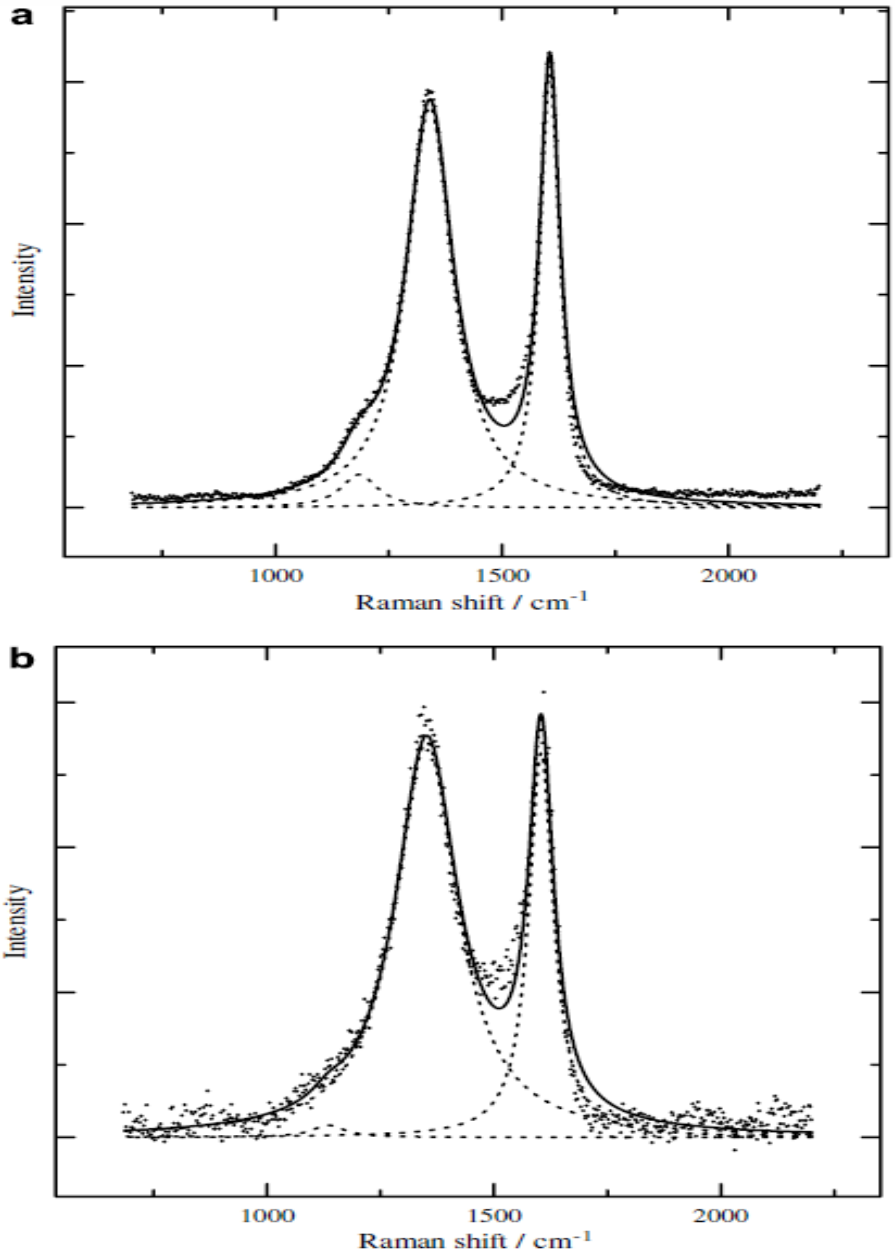

Fig. 5-4-3 Raman spectra of (a) pristine activated carbon fibers and (b) defluorinated ACFs.

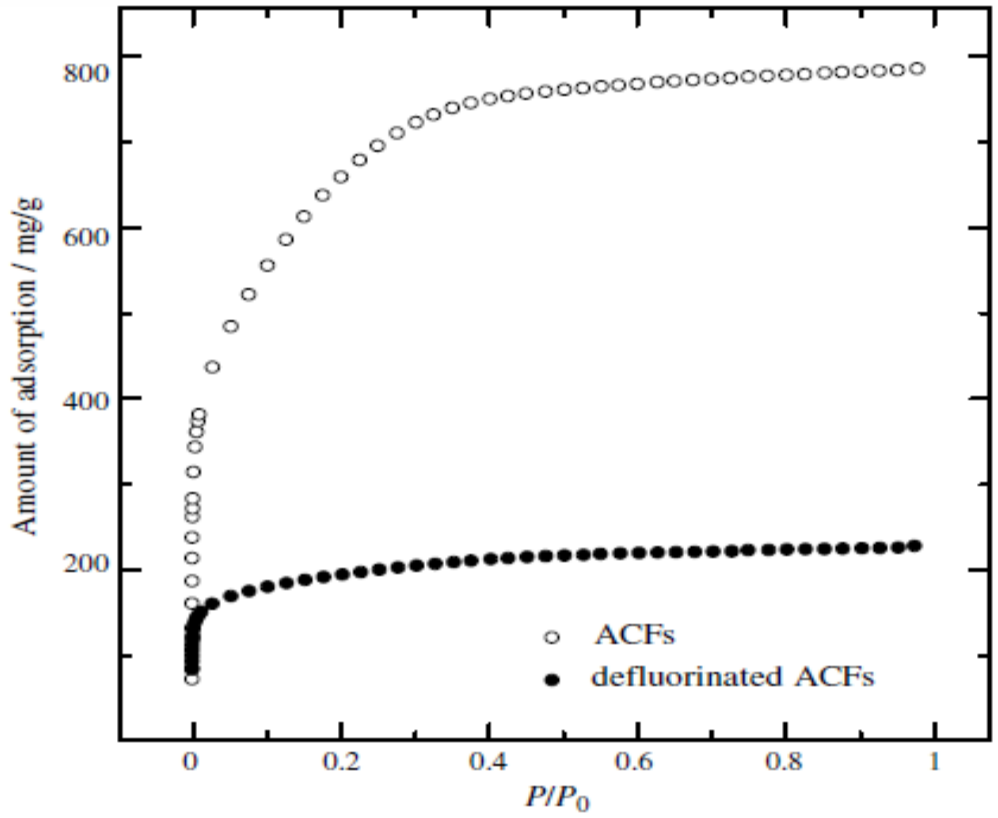

Fig. 5-4-4 Nitrogen adsorption isotherms of pristine activated carbon fibers (ACFs) and defluorinated ACFs at 77 K.

Table 5-4-1

Pore structural parameters of pristine activated carbon fibers (ACFs) and defluorinated ACFs. S_{BET}, W_0, $\Delta H_{iso,1/e}$, and w are BET surface area, micropore volume, isosteric heat of adsorption, and pore width, respectively

	S_{BET} (m^2/g)	W_0 (cm^3/g)	$\Delta H_{iso,1/e}$ (kJ/mol)	w (nm)
ACFs	1700	0.63	11.3	1.1
Defluorinated ACFs	660	0.22	12.8	0.8

The nitrogen adsorption isotherms of pristine and defluorinated ACFs are shown in Fig. 5-4-4. The pore parameters calculated from the nitrogen adsorption isotherms are listed in Table 5-4-1. A large decrease in the amount of nitrogen adsorbed on the defluorinated ACFs was observed. The average micropore widths of pristine and defluorinated ACFs were 1.1 and 0.8 nm, respectively, indicating the decrease in the

micropore width by defluorination. The isosteric heats of adsorption ($\Delta H_{iso,1/e}$) evaluated from Dubinin–Radushkevich (DR) analysis were 11.3 and 12.8 kJ/mol for pristine and defluorinated ACFs, respectively. The increase of $\Delta H_{iso,1/e}$ for defluorinated ACFs indicates an increase in the molecular potential of the nitrogen molecule in the micropores of defluorinated ACFs. These results suggest that the defluorinated ACFs have both narrower micropores and more local defective holes than pristine ACFs. Therefore, the defluorinated ACFs should possess both adsorption sites consisting of pores and defective holes having a stronger potential for interaction with hydrogen.

The adsorption isotherms of hydrogen at 77 K on pristine and defluorinated ACFs are shown in Fig. 5-4-5. Fig. 5-4-5a shows a decrease in the amount of hydrogen adsorption per unit mass (mg/g) on defluorinated ACF due to the decrease in the micropore volume by defluorination. However, the amount of hydrogen adsorbed by defluorinated ACF is larger than that of ACF at a low pressure range, suggesting that the defluorinated ACF has very small micropores. In Fig. 5-4-5b, the ordinate represents the amount of adsorbed hydrogen per micropore volume (mg/cm^3). The micropores of the defluorinated ACF adsorb more hydrogen than those of pristine ACF over the whole pressure range, indicating the enhancement of hydrogen adsorptivity on the micropores by defluorination. Defluorination leads to the narrowing of the micropores and an increase in defective holes embedded in the hexagonal lattice of micrographites. Narrowing the micropores strengthens the dispersion interaction between hydrogen and pore-walls. Rzepka et al. reported that the slit-like pores with a pore size (d) of 0.7 nm give the highest volumetric densities for hydrogen storage, according to GCMC simulations.[28] They indicated that the molecular potential becomes greater with a decrease in the d value. The model with d = 0.7 nm has a single potential minimum at

the center of the pore. At this pore size, only one adsorbed layer can be formed between the pore walls and thus the adsorption potential becomes much greater due to the overlapping of adsorption potential from opposing pore walls. Therefore, the volumetric capacity for hydrogen becomes higher with a decrease of micropore width from 1.1 nm to 0.8 nm by defluorination. As the defective holes in the micrographite should have an effective charge, the charge-induced dipole attractive interactions must add to the dispersion interaction, indicated on charged carbon nanotubes.[29] Thus defluorination gives rise to a remarkable enhancement of hydrogen adsorptivity on the micropores in ACFs. A future study needs to prove the existence and characteristics of the defective holes on defluorinated ACF, to further the design of a better porous carbon medium for hydrogen adsorption.

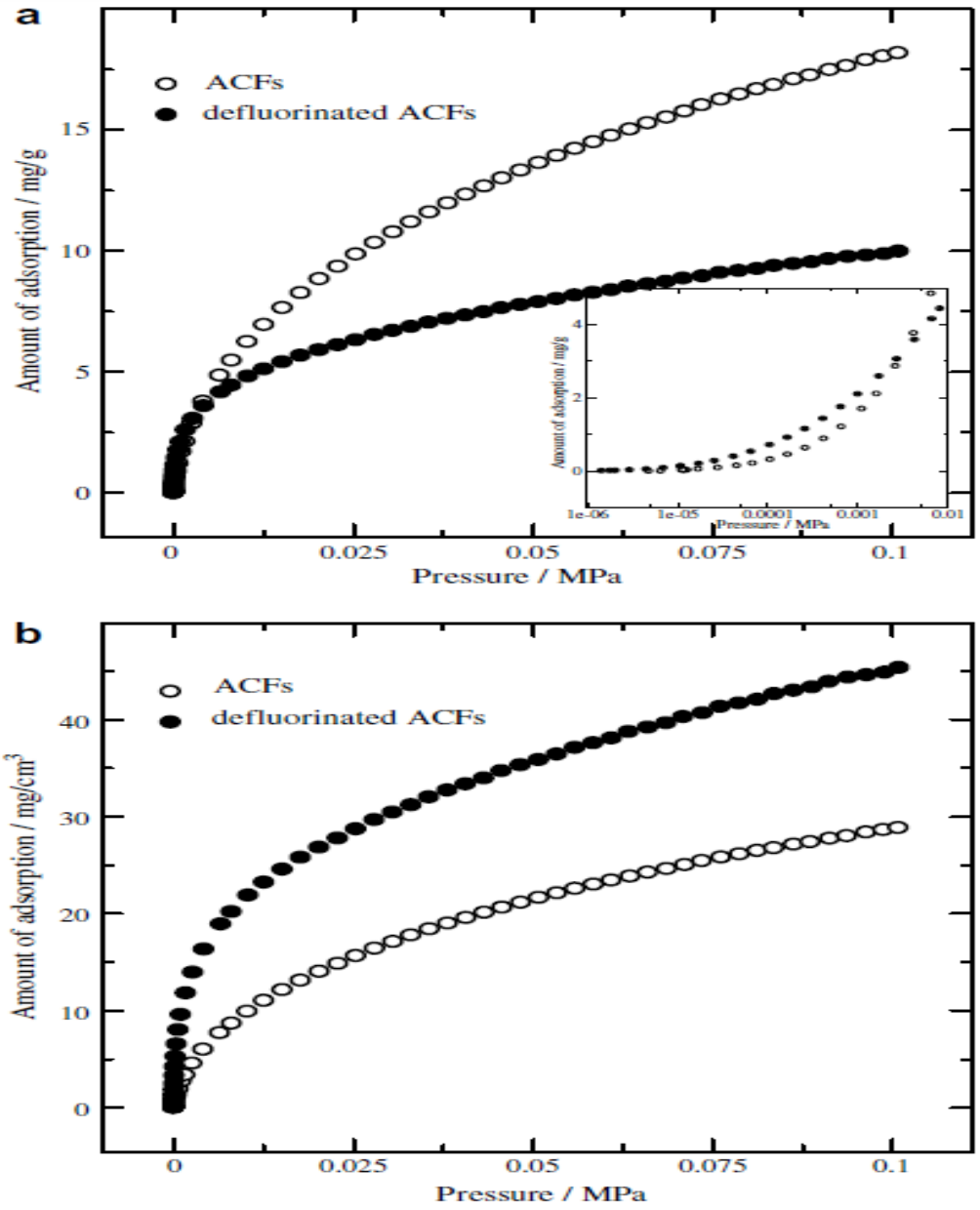

Fig. 5-4-5 Hydrogen adsorption isotherms of pristine ACFs and defluorinated ACFs at 77 K. The amount of adsorption is expressed as adsorbed hydrogen (a) per unit mass and (b) per micropore volume. The inset in (a) provides the isotherms at low pressure range.

References

(1) Dillon AC, Hebeb MJ. Hydrogen storage using carbon adsorbents: past, present and future. Appl Phys A 2001;72(2):133–42.

(2) Casa-Lillo MA, Lamari-Darkrim F, Cazorla-Amoro´ s D, Linares-Solano A. Hydrogen storage in activated carbons and activated carbon fibers. J Phys Chem B 2002;106(42):10930–4.

(3) Zhao XB, Xiao B, Fletcher AJ, Thomas KM. Hydrogen adsorption on functionalized nanoporous activated carbons. J Phys Chem B 2005;109(18):8880–8.

(4) Cheng H, Yang Q, Liu C. Hydrogen storage in carbon nanotubes.Carbon 2001;39(10):1447–54.

(5) Pan L, Sander MB, Huang X, Li J, Smith M, Bittner E, et al.Microporous metal organic materials: promising candidates as sorbents for hydrogen storage. J Am Chem Soc 2004;126(5):1308–9.

(6) Rowsell JLC, Millward AR, Park KS, Yaghi OM. Hydrogen sorption in functionalized metal-organic frameworks. J Am Chem Soc 2004;126(18):5666–7.

(7) Panella B, Hirscher M, Pu¨ tter H, Mu¨ ller U. Hydrogen adsorption in metal-organic frameworks: Cu-MOFs and Zn-MOFs compared. Adv Funct Mater 2006;16(4):520–4.

(8) Kaneko K. Molecular resolution analysis of a-FeOOH-dispersed activated carbon fibers. Langmuir 1991;7(1):109–15.

(9) Kaneko K. Determination of pore size and pore size distribution 1: adsorbents and catalysis. J Membrane Sci 1994;96(1–2):59–89. [10] Kaneko K. Molecular assembly formation in a solid nanospace. Colloid Surf A 1996;109:319–33.

(11) Kaneko K. Micropore filling mechanism in inorganic sorbents. Stud Surf Sci Catal 1996;99:573–98.

(12) Kaneko K. Heterogeneous surface structures of adsorbents. Stud Surf Sci Catal 1997;104:679–714.

(13) Kaneko K, Ishii C, Nagai N, Kanoh H, Hanzawa Y, Setoyama N, et al. Characterization of porous carbons with high resolution as analysis and low temperature magnetic susceptibility. Adv Colloid Interface Sci 1998;76–77:295–320.

(14) Kaneko K. Nanospace geometry sensitive molecular assembly. Supramolecular Sci 1998;5(3–4):267–73.

(15) Kaneko K. Control of supercritical gases with solid nanospace – environmental aspects. Stud Surf Sci Catal 1999;120B:635–57.

(16) Kaneko K. Specific intermolecular structures of gases confined in carbon

nanospace. Carbon 2000;38(2):287–303.
(17) Kaneko K, Ohba T, Ohkubo T, Utsumi S, Kanoh H, Yudasaka M, et al. Nanospace molecular science and adsorption. Adsorption 2005;11(1):21–8.
(18) Touhara H, Okino F. Property control of carbon materials by fluorination. Carbon 2000;38(2):241–67.
(19) Touhara H, Inahara J, Mizuno T, Yokoyama Y, Okamoto S, Yanagiuchi K, et al. Property control of new forms of carbon materials by fluorination. J Fluorine Chem 2002;114(2):181–8.
(20) Li G, Kaneko K, Ozeki S, Okino F, Ishikawa R, Kanda M, et al. Water rejective nature of fluorinated microporous carbon fibers. Langmuir 1995;11(3):716–7.
(21) Li G, Kaneko K, Okino F, Ishikawa R, Kanda M, Touhara H. Adsorption behaviour of polar molecules in fluorinated micropores. J Colloid Interface Sci 1995;172(2):539–40.
(22) Setoyama N, Li G, Kaneko K, Okino F, Ishikawa R, Kanda M, et al. Nitrogen adsorption on fluorinated activated carbon fiber. Adsorption 1996;2(4):293–7.
(23) Kaneko K, Setoyama N, Li G, Okino F, Ishikawa R, Kanda M, et al. Pore structures and adsorption properties of fluorinated activated carbon fibers. TANSO 1999;187:71–6.
(24) Takai K, Sato H, Enoki T, Yoshida N, Okino F, Touhara H. Effect of fluorination on nano-sized p-electron system. J Phys Soc Jpn 2001;70(1):175–85.
(25) Gu Z, Peng H, Hange RH, Smally RE, Magrave JL. Cutting singlewall carbon nanotubes through fluorination. Nano lett 2002;2(9):1009–13.
(26) Zhao W, Song C, Zheng B, Liu J, Viswanathan T. Thermal recovery behaviour of fluorinated single-walled carbon nanotubes. J Phys Chem B 2002;106(2):293–6.
(27) Pehrsson PE, Zhao W, Baldwin W, Song C, Liu J, Kooi S, et al. Thermal fluorination and annealing of single-wall carbon nanotubes. J Phys Chem B 2003;107(24):5690–5.
(28) Rzepka M, Lamp P, de la Casa-Lillo MA. Physisorption of hydrogen on microporous carbon and carbon nanotubes. J Phys Chem B 1998;102(52):10894–8.
(29) Simonyan VV, Diep P, Johnson JK. Molecular simulation of hydrogen adsorption in charged single-walled carbon nanotubes. J Chem Phys 1999;111(21):9778–83.

5-5 CO_2 Adsorption Properties of Activated Carbon Fibers under Ambient Conditions

5-5-1 Abstract CO_2 adsorption isotherms of activated carbon fiber (ACF) samples with different porosities were recorded at 273 and 298 K under ambient pressure for evaluation as a carbon capture and storage (CCS) technology. The porosities of the ACFs were characterized through N_2 adsorption at 77 K. The three types of ACFs tested, A5, A10, and A20, have different slit-shaped pore widths, specific surface areas, and micropore volumes. A5 contained ultramicropores and achieved a higher adsorption of CO_2 at low relative pressure (< 0.015) at 273 K. However, A10, which had an average pore width of 0.9 nm, exhibited the highest capacity of 195 mg g^{-1} at higher pressure of about 100 kPa, which is a relatively high value compared with that of conventional activated carbon. By establishing the temperature dependence of CO_2 adsorptivity and employing Dubinin-Radushkevich analysis, we characterized the interaction energy between pores and CO_2 molecules. Our results shed light on fundamental aspects of CO_2 adsorption of ACFs, moving them toward being a viable CCS.

5-5-2 Introduction

Carbon capture and storage (CCS) will play an important role in reducing greenhouse gas emission levels in the atmosphere in the effort to avoid permanent and irreversible damage to the ecological system caused by the use of fossil fuels. Chemical absorption using amines is currently employed for CO_2 separation in industrial processes such as the sweetening of natural gas, and hydrogen or ammonia production, and is considered to be the most ready-to-use technology for post-combustion CO_2 capture. However, this technology in its present state has a number of drawbacks, such

as the high energy requirement associated with sorbent regeneration, amine losses due to evaporation, corrosion, and thermal and chemical degradation of the amines in the presence of oxygen.[1)] Because of these problems, adsorption as a separation technology has the potential to reduce the cost of post-combustion capture when compared to amine scrubbing.

Zeolite13X is the adsorbent most extensively studied in CO_2 separation processes because of its high selectivity for CO_2.[2)] However, several studies have also appeared in the literature examining activated carbons,[3)] which present important advantages over zeolites, such as greater hydrophobicity, significantly lower cost, and lower energy requirements for regeneration.

CO_2 adsorption has been used to evaluate narrower micropores in microporous materials (Rodríguez-Reinoso *et al.* 1989; Lozano-Castelló *et al.* 2004).[4,5)] However, studies assessing the applicability of activated carbons as a CO_2 adsorbent under ambient conditions began only relatively recently as evidenced by the small number of relevant references in the literature. CO_2 adsorptivity of carbide-derived carbons with different pore sizes has been examined in detail,[3)] and carbon molecular sieves have been found to exhibit high CO_2 adsorptivity.[6,7)] Activated carbon fibers (ACFs) are so widely-used and commercialized that their physicochemical properties of ACFs are relatively well-defined. Studying the CO_2 adsorptivity of ACFs will promote the use of activated carbons as a CCS technology.

In this section, we systematically examined CO_2 adsorption isotherms of different activated carbon fibers (ACFs) at 273 and 298 K under ambient pressure to gather fundamental data useful for evaluating them as a CCS technology.

5-3 Experimentals

Pitch-based activated carbon fibers, A5, A10, and A20, were supplied from AD'ALL Co. Ltd. and used as adsorbents. The ACFs were pretreated at 423 K under vacuum for 2 hours before adsorption experiments. Adsorption isotherms of N_2 at 77 K were collected using an AUTOSORB-1-MP (Quantachrome Instruments) and adsorption isotherms of CO_2 at 273 and 298 K were measured with AUTOSORB-iQ (Quantachrome Instruments) and BELSORP Mini (BEL Japan, Inc.).

5-4 Results and Discussion

The porosities of the three different types of ACFs were characterized via N_2 and CO_2 adsorption isotherms at 77 K and 273 K, respectively. Fig. 5-5-1 shows the N_2 adsorption isotherms at 77 K. The three isotherms are of type I, indicating the presence of micropores in the ACFs; these results indicate that A5 and A10 have narrower micropores than does A20, as appreciable uptakes was observed at very low relative pressure ($<10^{-5}$) in the isotherms for A5 and A10. The isotherms were analyzed by using α_s plots.[8] The pore parameters are summarized in Table 5-5-1. The average pore width for each sample was calculated by assuming a regular slit-shaped pore for the ACFs.

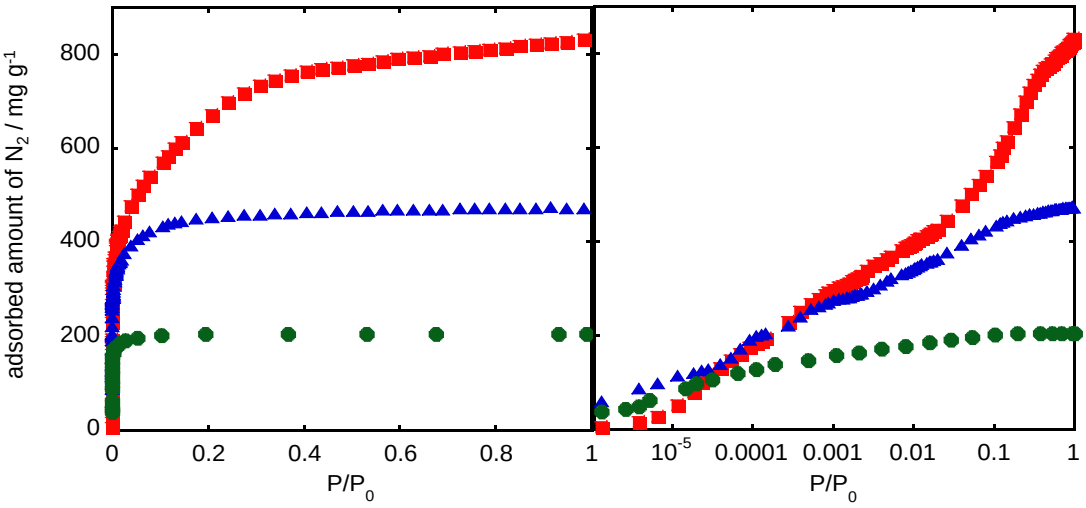

Fig. 5-5-1 N_2 adsorption isotherms of ACFs: ●, A5; ▲, A10; ■, A20
Left: linear plot, Right: semi-l

Table 5-5-1 Pore parameters of ACFs obtained from N_2 adsorption isotherms at 77 K

	pore width / nm	specific surface area / $m^2\ g^{-1}$	micropore volume / $cm^3\ g^{-1}$
A5	0.64	780	0.25
A10	0.86	1140	0.49
A20	1.09	1650	0.90

The CO_2 adsorption isotherms at 273 K also reflect the porosities of each sample. Higher adsorption was observed for A5 at $P/P_0 < 0.015$ (Fig. 5-5-2), which arises from the narrower pore width of A5 and agrees well with the known order of pore width, A5 < A10 < A20. However, under higher relative pressure, the amount of CO_2 adsorbed on A10 was greater than that on A5 because of its greater pore volume, which plays an important role in saturation capacity. The CO_2 adsorptivity of A10 and A20 tended to increase above $P/P_0 > 0.03$ because of their greater micropore volume, although the CO_2 adsorption of A5 is was nearly saturated at that pressure. 195 mg g^{-1} of CO_2 adsorbed on A10 at 273 K and 100 kPa is a relatively large amount compared with amounts adsorbed by conventional activated carbons,[5,9-11] although carbide-derived carbons and carbon molecular sieves exhibit even higher CO_2 adsorptivities.[3,6,7]

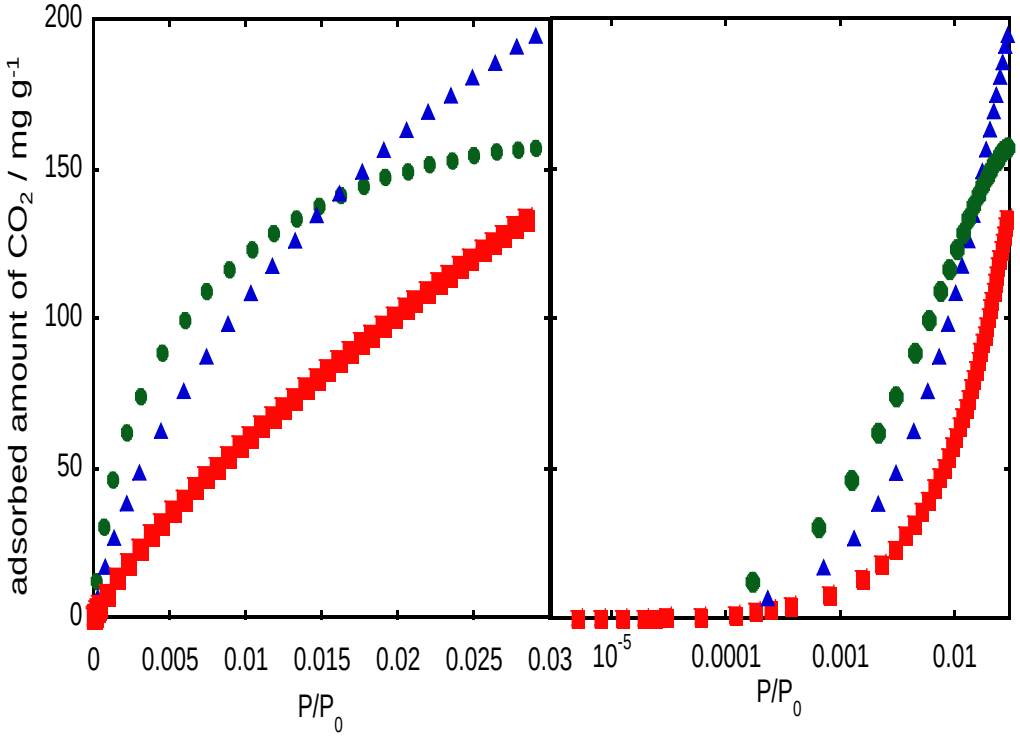

Fig. 5-5-2 CO_2 adsorption isotherms of ACFs at 273 K:
●, A5; ▲, A10; ■, A20
Left: linear plot, Right: semi-log plot

The temperature dependence of CO_2 adsorptivity of the ACFs was also examined. The resulting isotherms at 273 K and 298 K are shown in Fig. 5-5-3. The three isotherms at 298 K have similar shapes to those collected at 273 K. However, the amounts of adsorbed CO_2 are lower than those at 273 K because of physical adsorption. In particular, the isotherm of A5 at 298 K shows a marked decrease in the amount of

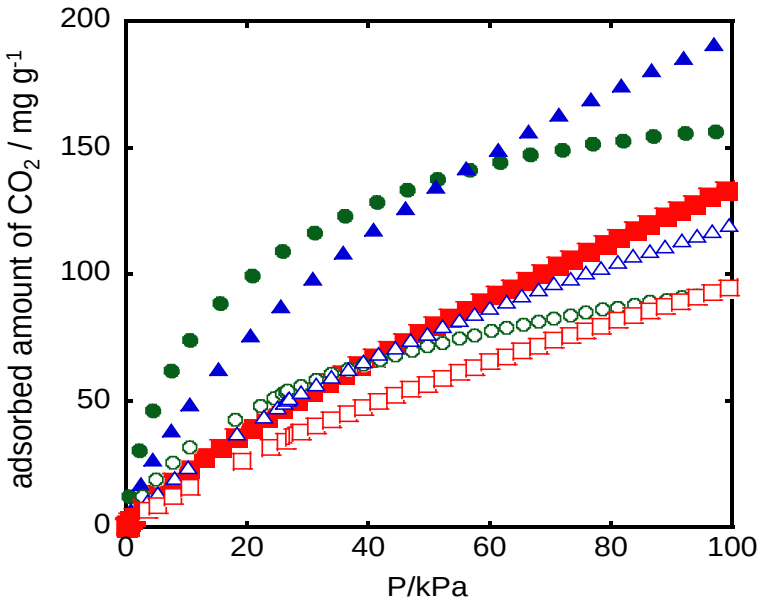

Fig. 5-5-3 CO_2 adsorption isotherms of ACFs: circles, A5; triangles, A10; squares, A20. Closed: 273 K, Open: 298 K

adsorbed CO_2, suggesting the greater temperature dependence. By applying the Clausius-Clapeyron equation to these adsorption data, the isosteric heat (q_{st}) values of CO_2 adsorption of the three ACFs were obtained (Fig. 5-5-4).

As expected from the temperature dependence observed in the data in Fig. 5-5-3 and the adsorption potential related to pore width, A5 indicated the highest q_{st} value > 40 kJ mol^{-1}. The q_{st} value for A10 was smaller than that for A5 and similar to ΔH of

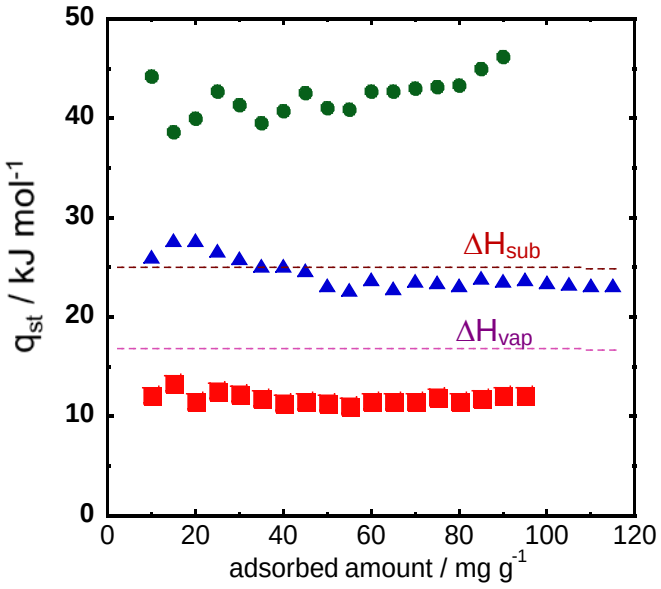

Fig. 5-5-4 Isosteric heat (q_{st}) of CO_2 on ACFs: ●, A5; ▲, A10; ■, A20
Brown and purple dashed lines: Enthalpy changes of sublimation (ΔH_{sub}) and vaporization (ΔH_{vap}) of CO_2, respectively.

sublimation of CO_2 and that for A20 was lower than ΔH of the vaporization of CO_2. The dependence of q_{st} on the amount of CO_2 adsorbed is modest and nearly constant, although the data for A5 are not as tight and those for A10 gradually decrease with increasing CO_2 adsorption. The desorptivity is also an important consideration for practical use. A5 exhibited perfect reversibility as indicated through its desorption isotherm, even though its q_{st} value is > 40 kJ mol^{-1}. Some kinds of zeolite require large amounts of energy to regenerate and desorb CO_2 molecules because the interactions are so strong,[7,12] but ACFs require only a decrease in CO_2 pressure at room temperature.

Table 5-5-2 Dubinin-Radushkevich parameters of ACFs obtained from N_2 and CO_2 adsorption isotherms

N_2	A5	A10	A20
W_0 / mg g^{-1}	202	424	780
βE_0 / kJ mol^{-1}	8.7	6.4	6.0
CO_2	A5	A10	A20
W_0 / mg g^{-1}	300	365	265
βE_0 / kJ mol^{-1}	11.1	9.3	8.5

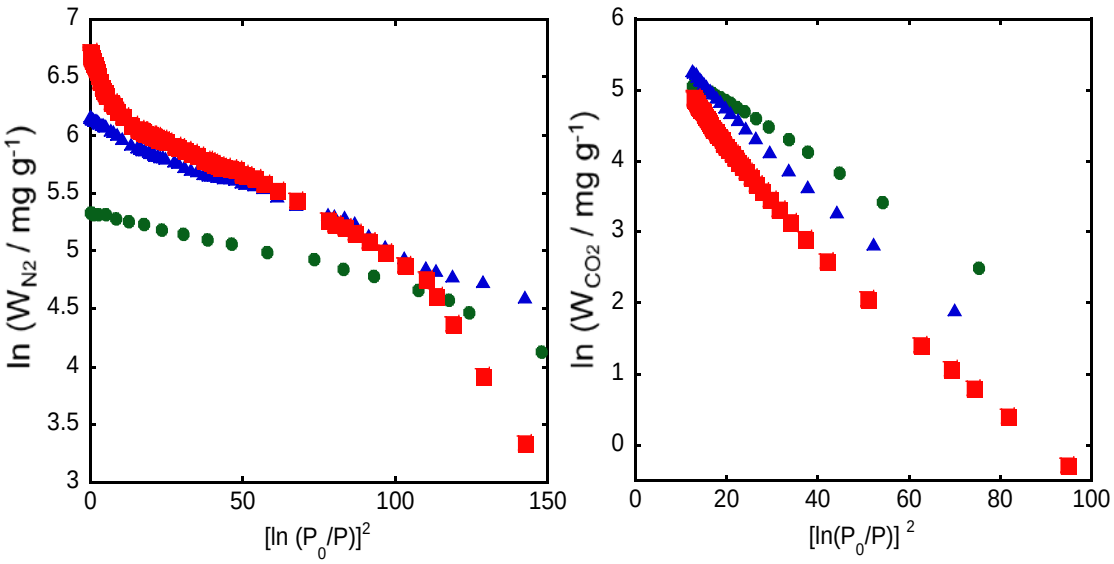

Fig. 5-5-5 Dubinin-Radushkevich plots of N_2 (left) and CO_2 (right) adsorption: ●, A5; ▲, A10; ■, A20

To compare microporosity of the ACFs, the Dubinin-Radushekevich (DR) equation

($\ln(W/W_0) = -(RT/\beta E_0)^2[\ln(P_0/P)]^2$) was applied to the isotherm data, where W, W_0, β, and E_0 are the amount of adsorbed CO_2, the saturation amount, the affinity coefficient,and the characteristic energy, respectively. Fig. 5-5-5 shows the DR plots for N_2 adsorption at 77 K and CO_2 adsorption at 273 K. The curves for A5 and A10 in the N_2 adsorption isotherms at 77 K exhibit better linearity in the range of $[\ln(P_0/P)]^2$ than does A20, which possesses a smaller amount of narrower micropores and a larger amount of wider pores. In contrast, the curves for all three ACFs show good linearity for CO_2 adsorption at 273 K. Using the linear portion from 20 to 50 of $[\ln(P_0/P)]^2$ for each curve, W_0 and βE_0 were evaluated and the results are summarized in Table 2. The βE_0 value reflects the strength of the interaction potential between pores and molecules and was found to decrease (A5 > A10 > A20) with increasing pore width in both adsorption isotherms. The βE_0 of A5 for CO_2 adsorption was remarkably large, leading to $q_{st \text{ at } \phi=e^{-1}}$ = 28 kJ mol^{-1}, where ϕ is fractional filling. However, the W_0 value for N_2 adsorption for the three ACFs was different from that for CO_2 adsorption. Since A5 has more ultramicropores and A20 contains relatively larger pores, W_0 of A5 in CO_2 adsorption was larger than that of A20 while the opposite is true for N_2 adsorption at 77 K. Thus, the CO_2 adsorptivity of commercial ACFs can be understood from the viewpoint of pore parameters such as pore width.

5-5 Conclusions

The CO_2 adsorptivity of commercial pitch-based ACFs with different pore widths were examined under ambient conditions. Under very low CO_2 pressure, the ACF featuring ultramicropores exhibited high adsorptivity while the sample with an average pore width of 0.9 nm exhibited the highest adsorptivity (195 mg g^{-1}) at 100 kPa. The

interaction between the pores and CO_2 molecules was elucidated by analyzing the temperature dependence of adsorptivity and the related Dubinin-Radushkevich plots. It is likely that certain mixtures of these ACFs will exhibit optimum adsorptivity of CO_2 for each individual adsorption system and set of condition. Our results provide useful information for the practical use of commercial ACFs as a CCS technology.

References

(1) Plaza, M. G., García, S., Rubiera, F., Pis, J. J. and Pevida, C., *Chem. Eng. J.*, **2010**, 163, 41-47.

(2) Cavenati, S., Grande, C.A., and Rodrigues, A. E., *J. Chem. Eng. Data*, **2004**,1095-1101.

(3) Presser, V., McDonough, J., Yeon, S.-H. and Gogotsi, Y., *Energy Environ. Sci.*, **2011**, 4, 3059-3066.

(4) Rodríguez-Reinoso, F., Garrido, J., Martin-Martínez, J. M., Molina-Sabio, M. and Torregrosa, R., *Carbon*, **1989**, 27, 23-32.

(5) Lozano-Castelló, D., Cazorla-Amorós, D. and Linares-Solano, A., *Carbon*, **2004**, 42, 1233-1242.

(6) Wahby, A., Ramos-Fernández, J., Martínez-Escandell, M., Sepúlveda-Escribano, A., Silvestre-Albero, J., Rodríguez-Reinoso, F., *ChemSusChem*, **2010**, 3, 974-981.

(7) Silvestre-Albero, J., Wahby, A., Sepúlveda-Escribano, A., Martínez-Escandell, M., Kaneko K., Rodríguez-Reinoso, F., *Chem. Commun.*, **2011**, 47, 6840-6842.

(8) Kaneko, K., *J. Membrane Sci.*, **1994**, 96, 59-89.

(9) Sun, Y., Wang, Y., Zhang, Y., Zhou Y. and Zhou, L., *Chem. Phys. Lett.*, **2007**, 437, 14-16.

(10) Ravikovitch, P. I. and Neimark, A. V., *Adsorption*, **2005**, 11, 265-270.

(11) Blanco López, M. C., Martínez-Alonso, A. and Tascón, J. M. D., *Carbon*, **2000**, 38,1177-1182.

(12) Chue, K. T., Kim, J. N., Yoo, Y. J., Cho, S. H. and Yang R. T., *Ind. Eng. Chem. Res.*, **1995**, 34, 591-598.

6. General Conclusions

The effectiveness of the carbon dioxide capture and storage (CCS) in global warming countermeasures is recognized internationally and the study that capturing CO_2 artificially and storage are promoted. As a method of CCS, chemical absorption with amines and adsorption by the zeolite are researched and developed. However, high energy requires to regeneration processes to separate CO_2 in the CCS methods.

In this study, CO_2 adsorption isotherms of different pitch-based activated carbon fibers were measured at 273 and 298 K under ambient pressure. In high pressure (100kPa) of CO_2, ACF of the pore width of 0.9 nm indicate high adsorbed amount as 195mg/g, on the other hand, under the low pressure of CO_2, the ACF of ultramicropores showed a higher adsorptivity.

The interaction between the pores and CO_2 molecules could be analyzed by the temperature dependence of adsorptivity and DR plots.

By mixing ACFs, some mixtures have better adsorptivity of CO_2 according to change of the adsorption condition. The data obtained in this study will supply some useful information for the field of CCS. Currently, as for the chemical absorption with amines which is used in industrial process generally, there are some drawbacks, such as high energy require to reproduction and amine losses due to evaporation. Zeolite13X is studied widely in CO_2 separation processes because of its high selectivity to CO_2, but has a problem to need much energy for reproduction. The method using activated carbons enable reproduction at lower cost due to its temperature dependence, as showed partly in this study. By the characteristic of ACF, the

adsorptivity at the low-concentration range is superior to a granulated active carbon, and the optimization by the combination with other methods is possible. Combining the process using activated carbon fibers with the existing processes, enable us more effective system.

The data obtained in this study will supply useful information for practical use of activated carbon fiber for the CCS technology.

Acknowledgement

To conduct this research, I am deeply grateful to Professor Hirofumi Kanoh for his considerable supervisions throughout this research.

To conduct this research, I also appreciate Assistant Professor Dr. Tomonori Ohba to give advices and bring corporation help.

Also to conduct this research, I deeply appreciate Masumi Baba to work together cooperatively.

Also to conduct this research, I deeply express my appreciation to everyone from Kanoh laboratory foe their supervisions, advices and cooperation throughout this area.

To advance this research, I appreciate everyone from Malvern division for corporation of provided data.

January, 2013

Yoshitaka Nakahigashi

List of Publications

1) Yoshiyuki Hattori, Hideki Tanaka, Fujio Okino, Hidekazu Touhara, Yoshitaka Nakahigashi, Shigenori Utsumi, Hirofumi Kanoh, and Katsumi Kaneko
Quantum Sieving Effect of Modified Activated Carbon Fibers on H_2 and D_2 Adsorption at 20K, *J. Phys. Chem. B*, **2006**,110 (20), 9764-9767.
2) Yoshiyuki Hattori, Natsuko Noguchi, Fujio Okino, Hidekazu Touhara, Yoshitaka Nakahigashi, Shigenori Utsumi, Hideki Tanaka, Hirofumi Kanoh, Katsumi Kaneko
Defiuorination-enhanced hydrogen adsoptivity of activated carbon fibers
Carbon, **2007**, 45 (7), 1391-1395.
3) Yoshitaka Nakahigashi, Hiofumi Kanoh, Tomonori Ohba, Masumi Baba, Yoshiyuki Hattori, Naoya Inoue, and Masafumi Morimoto
CO_2 Adsorption Properties of Activated Carbon Fibers under Ambient Conditions
Ads. Sci. Technol., **30** (7), 621-626 (2012).